JOURNAL OF GEOPHYSICAL RESEARCH, VOL. 111, D18306, doi:10.1029/2005JD006516, 2006

Multiscale modeling of air pollutants dynamics in the northwestern Mediterranean basin during a typical summertime episode

Pedro Jiménez,[1] Jos Lelieveld,[2] and José M. Baldasano[1]

Received 19 July 2005; revised 7 March 2006; accepted 1 June 2006; published 26 September 2006.

[1] The complex behavior of photochemical pollutants in the northwestern Mediterranean basin (NWMB) is conditioned by the superposition of circulations of different scale and the pattern of emissions. Therefore a new approach to the modeling of air quality in the NWMB has been adopted by combining the global climate-chemistry model ECHAM5/MESSy and the regional modeling system MM5-EMICAT2000-CMAQ to analyze the high levels of photochemical air pollution during a typical summertime episode. We show that this combination of models is well suited to address the range of scales involved. The complexity of the area requires the application of high spatial and temporal resolution (2 km and 1 hour) modeling to cover local to regional interactions. We address the local and large-scale processes controlling tropospheric ozone in the NWMB, notably emissions and photochemistry, convective and advective transport, deposition processes, and stratosphere-troposphere exchange. The simulation results indicate that the ozone buildup largely results from local photochemical production, which strongly exceeds the removal rates through transport and deposition. The contribution by advective transport is limited, associated with the stagnant meteorological conditions. In the lower troposphere, local recirculation systems are of key importance. The strength of the land-sea breeze circulation and thermally or mechanically driven convection over the complex orography of the eastern Iberian coast can induce vertical transport and the layering of air pollution.

Citation: Jiménez, P., J. Lelieveld, and J. M. Baldasano (2006), Multiscale modeling of air pollutants dynamics in the northwestern Mediterranean basin during a typical summertime episode, *J. Geophys. Res.*, *111*, D18306, doi:10.1029/2005JD006516.

1. Introduction

[2] The high levels of photochemical pollutants (especially ozone, O_3) over the northwestern Mediterranean basin (NWMB) in summer influence natural ecosystems, agriculture and human health. The cloud-free conditions and high solar radiation intensity promote the photochemical buildup of ozone and other pollutants [*Lelieveld et al.*, 2002]. Measurements have shown high O_3 concentrations in this Mediterranean region [e.g., *Ziomas et al.*, 1998; *Millán et al.*, 2000; *Dueñas et al.*, 2002]. According to *Ribas and Peñuelas* [2004], the European Union human and plant protection thresholds are exceeded in the NWMB on 54 and 297 days per year, respectively. Atmospheric chemistry transport model simulations suggest that summertime O_3 is enhanced in the entire Mediterranean troposphere, contributing substantially to the radiative forcing of climate [*Lawrence et al.*, 1999; *Hauglustaine and Brasseur*, 2001]. Furthermore, the concentrations of airborne particulate matter and ozone are related in the NWMB. Both pollutant categories undergo seasonal variations characterized by a summer maximum [*Jiménez et al.*, 2003a]. The levels of primary and secondary pollutants reported by air quality stations indicate a clear relationship when relating seasonal PM_{10} and O_3 concentration at ground level (correlation coefficient of 0.87 during the summer months). Simultaneous peak concentrations of PM_{10} and O_3 measured at surface stations corresponded to a vertical distribution of aerosols in multiple layers with variable thickness above the mixing layer as detected by the lidar station of Barcelona [*Pérez et al.*, 2004].

[3] The pronounced topography of the NWMB induces a complex flow regime associated with the development of mesoscale phenomena that interact with the synoptic flow. Local orographical and land-sea breezes have important consequences for the dispersion of pollution emissions, especially during summer. The nonhomogeneity of the terrain, the diverse land use and the different types of vegetation contribute to locally specific conditions. In fact, the flow structure is rather complicated because of the superposition of atmospheric circulations on a range of different scales.

[4] Some authors point to the similarities between the NWMB and the Southern California Air Basin (SoCAB), affected by a factor of scale [*Barros et al.*, 2003; *Pérez et al.*, 2004]. For instance, the structure of the sea-land breeze, the presence of elevated pollution layers and the formation of the thermal internal boundary layer have been studied in locations such as Los Angeles [*Wakimoto and McElroy*, 1986; *Liu et al.*, 1987; *Boucouvala and Bornstein*, 2003] and Barcelona

[1] Barcelona Supercomputing Center–Centro Nacional de Supercomputación, Barcelona, Spain.
[2] Department of Atmospheric Chemistry, Max Planck Institute for Chemistry, Mainz, Germany.

0148-0227/06/2005JD006516$09.00

[*Soriano et al.*, 2001; *Pérez et al.*, 2004]. *McElroy and Smith* [1993] and *Dabdub et al.* [1999] examined the creation and fate of ozone in the SoCAB. Layers aloft were attributed to the action of slope flows (including convergence), convective elements transported into the inversion layer and undercutting by the sea breeze flow. High levels of ozone were found along the slopes of the surrounding mountain barriers and in the eastern basin [*Lu and Turco*, 1996]. Vertical circulations associated with the interaction of the sea breeze and mountain slope winds inject pollutants into the base of the inversion and create high concentrations of pollutants; but in the case of Los Angeles, the presence of a hot desert laying to the east of the mountain barriers promotes vertical injections with a thermal cause [*Jacobson*, 2002], while in the NWMB this vertical injection is promoted by the precoastal mountain range.

[5] A number of studies have shown that during typical summertime conditions, layering and accumulation of pollutants such as ozone and aerosols were taking place along the eastern coast of the Iberian Peninsula. The European projects MECAPIP; Mesometeorological Cycles of Air Pollution in the Iberian Peninsula (1988–1991), and RECAPMA; Regional Cycles of Air Pollutants in the western Mediterranean area (1990–1992) characterized the meteorological conditions and mesoscale transport mechanisms over the Iberian Peninsula and the western Mediterranean mainly from experimental campaigns [*Millán et al.*, 1992, 1996, 1997, 2000]. Recently, the project ESCOMPTE; Expérience sur Site pour Contraindre les Modèles de Pollution atmosphérique et de Transport d'Emissions program included atmospheric emission inventories and field experiments in the northwestern Mediterranean region (southern France) to show the high occurrence of photochemical pollution events. The results of ESCOMPTE in southern France highlighted the dynamical characteristics of the area. Sea breeze circulation and channeling effects due to terrain features strongly influence the location of the pollutant plumes [*Cros et al.*, 2004; *Cousin et al.*, 2005; *Dufour et al.*, 2005; *Lasry et al.*, 2005; *Kalthoff et al.*, 2005; *Ancellet and Ravetta*, 2005; *Coll et al.*, 2005].

[6] However, there is a need for modeling studies for the specific area of the NWMB that take into account the superposition of circulations of different scales in long stagnant periods leading to episodes of air pollution. This type of studies can provide a three-dimensional high-resolution description of the dynamics of atmospheric pollutants over this very complex area. The aim of this work is to study the contributions of different physico-chemical processes to tropospheric O_3 in the NWMB, combining a global and a regional model applied with high spatial and temporal resolution (2 km and 1 hour), to explain the high levels of photochemical air pollution in this area during summer.

[7] The episode of 13–16 August 2000 was selected to perform the simulations, since it represents a typical weather pattern over the Mediterranean area in summer during which pressure gradients are small [*Jorba et al.*, 2004]. We have performed an evaluation of ECHAM5/MESSy and MM5-EMICAT2000-CMAQ using a large surface database from air quality stations in the NWMB. In addition, Lidar vertical profiles from *Pérez et al.* [2004] have been used to evaluate the model calculations of vertical layering over the NWMB. We have discriminated and quantified the different processes by subdividing the troposphere into three different altitude layers, the lower, middle and upper troposphere, to facilitate the description and analysis of the phenomena involved. We quantify the tropospheric O_3 and carbon monoxide (CO) budgets over the NWMB, distinguishing (1) emissions and photochemistry, (2) convective transport, (3) advective transport, (4) dry and wet deposition, and (5) stratosphere-troposphere exchange (STE).

2. Methods

[8] Model simulations have been conducted for the photochemical pollution event over the NWMB on 13–16 August 2000. During this event the European Directive 2002/3/EC threshold for ground-level O_3 (180 $\mu g\ m^{-3}$ in 1 hour) was exceeded. The domain of study (D4) (Figure 1) covers an area of $272 \times 272\ km^2$ centered over the NWMB. This domain was extended through the ECHAM5/MESSy simulations for a domain covering most of Europe and the entire western Mediterranean area. The episode of 13–16 August 2000, corresponds to a typical summertime low-pressure gradient with high levels of photochemical pollutants over the area. These days were characterized by a weak synoptic forcing, so that mesoscale phenomena, induced by the particular geography of the region may be expected to be dominant. A high sea level pressure and negligible surface pressure gradients over the domain characterize this day, with low northwesterlies aloft (Figure 2). The selection of the episode is justified by the analysis of *Jorba et al.* [2004], who apply an objective multivariate statistical technique designed to explore structures within a data set covering 5 years. This nonhierarchical clustering algorithm specially designed for large databases has been used for the selection of the episode, since it allows obtaining flow climatology. The situation of 13–16 August 2000 is representative of episodes of photochemical pollution in the NWMB, since these conditions dominate 45% of the annual and 78% of the summertime transport patterns over the area of study. These conditions are associated with local-to-regional episodes of air pollution associated with high levels of O_3 during summer [*Toll and Baldasano*, 2000; *Barros et al.*, 2003]. Maximum O_3 levels over the NWMB were measured in the Vic and Alcover industrial zones ($189\ \mu g\ m^{-3}$).

[9] Two complementing approaches were used to describe the processes controlling the formation of photochemical pollutants in the NWMB. The general circulation model (GCM) applied in this study is the European Centre Hamburg Model version 5 (ECHAM5), coupled with a description of atmospheric chemistry, to study processes at a regional-global scale. For a more detailed description of local and mesoscale dynamical processes the MM5-EMICAT2000-CMAQ modeling system was used.

2.1. European Centre Hamburg Model Version 5 (ECHAM5)

[10] The ECHAM5 model [*Roeckner et al.*, 2003] was used at a horizontal resolution of about $1.8° \times 1.8°$ and a time step of 900 s (T63). ECHAM5 has been coupled to the Modular Earth Submodel System (MESSy) [*Jöckel et al.*, 2005], a generalized interface and submodel structure, which simulates large-scale chemistry-dynamics interactions by extending ECHAM5 into a fully coupled chemistry-climate

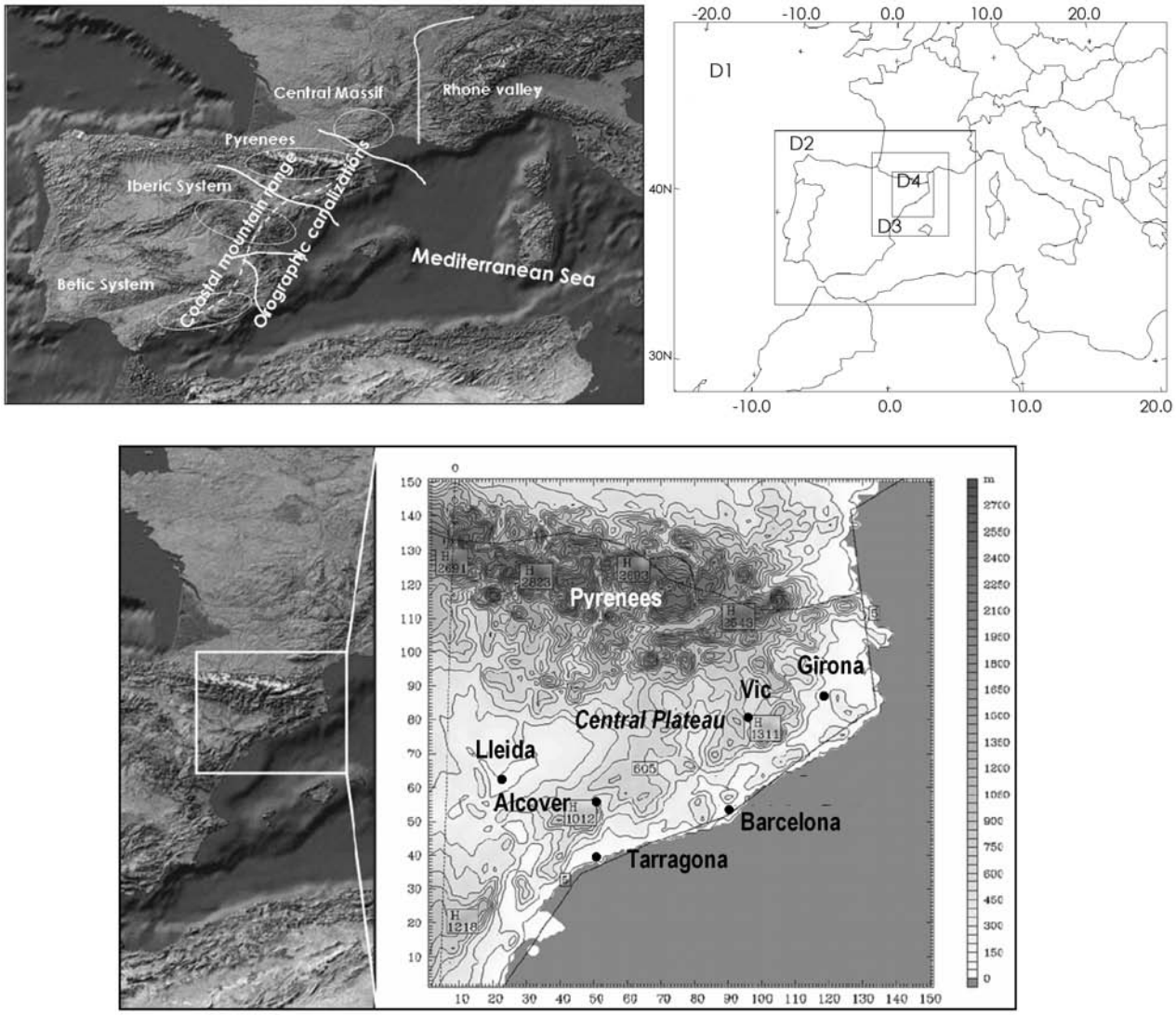

Figure 1. (top left) Northwestern Mediterranean basin (NWMB), (top right) nested domains and (bottom) topographical features in the area of study.

model. The model version used distinguishes 31 hybrid sigma-pressure layers between the surface and the top level at 10 hPa. Tracer transport is calculated with a flux form semi-Lagrangian advection scheme [*Lin and Rood*, 1996]. Additional vertical transports are included through the parameterization of vertical diffusion and convection.

[11] The model considers a separate stratospheric O_3 tracer, referred to as O_3s. The concentration of O_3s is equal to that of O_3 in the grid cells above the tropopause where stratospheric O_3 is prescribed [*Roelofs and Lelieveld*, 2000]. O_3s is transported from the stratosphere into the troposphere along with the calculated air motions [*Kentarchos and Roelofs*, 2003], where it is photochemically destroyed or removed by dry deposition. The difference between O_3 and O_3s is a measure of O_3 originating from photochemical production in the troposphere (O_3t).

[12] The representation of emissions is an essential component of the ECHAM5/MESSy chemistry-climate model. Emission inventories were derived from the EDGAR 3.2 database (http://arch.rivm.nl/env/int/coredata/edgar/), based on the work by *van Aardenne et al.* [2001]. The MECCA (Module Efficiently Calculating the Chemistry of the Atmosphere) chemistry model was coupled to ECHAM5 through the MESSy interface [*Sander et al.*, 2005]. The current mechanism of MECCA consists of five contributions: (1) tropospheric chemistry adapted from *von Kuhlmann et al.* [2003], (2) the chemical mechanism for the stratosphere adapted from *Steil et al.* [1998], and (3) tropospheric halogen and sulphur chemistry from *Sander and Crutzen* [1996] and *von Glasow et al.* [2002].

2.2. MM5-EMICAT2000-CMAQ

[13] The MM5 numerical weather prediction model [*Dudhia*, 1993] has been used to provide the meteorology dynamical parameters. The MM5 options used for the simulations were: Mellor-Yamada scheme as used in the Eta model for the planetary boundary layer (PBL) parameterization; Anthes-Kuo and Kain-Fritsch cumulus scheme;

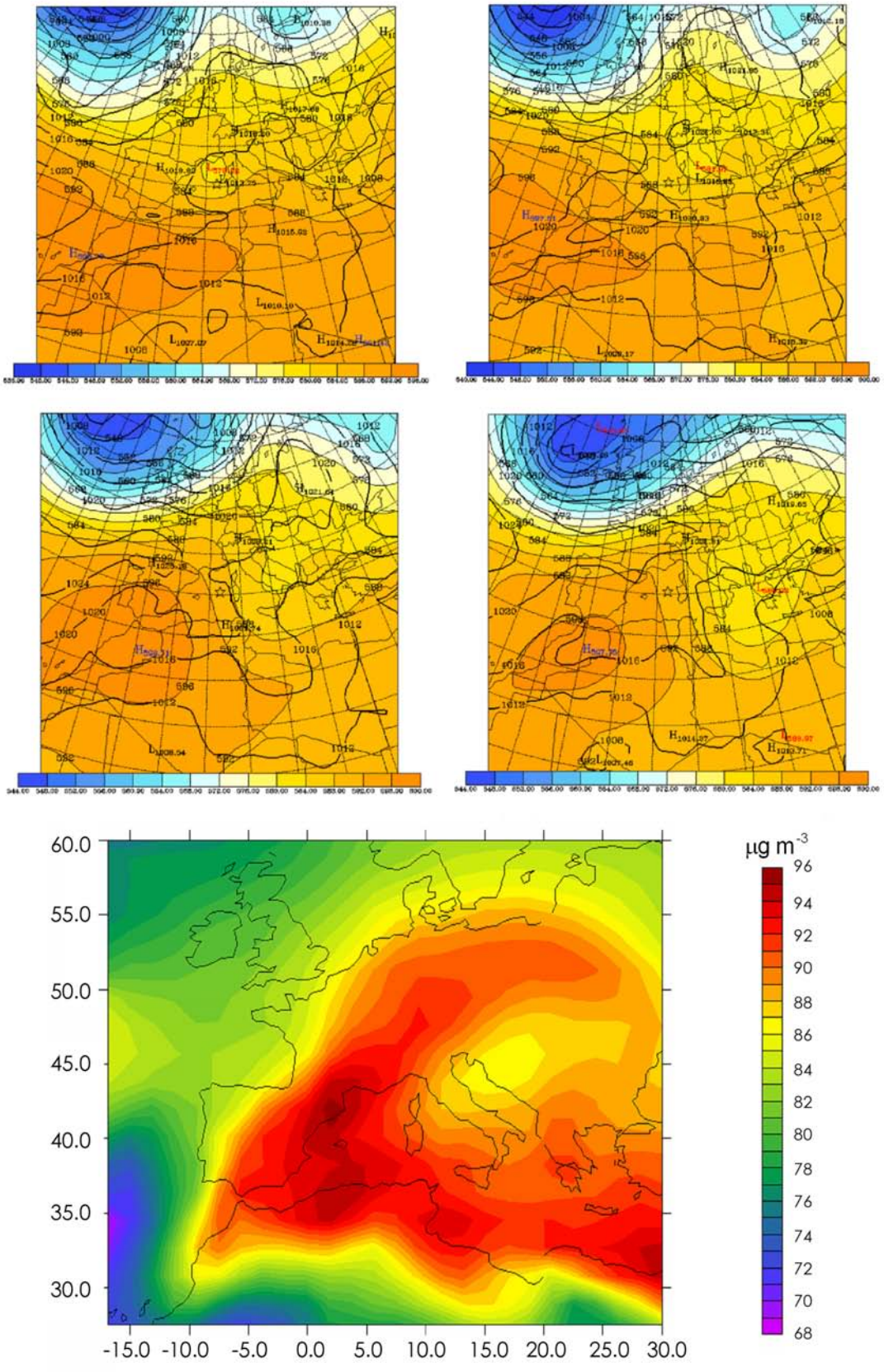

Figure 2. Synoptic situation of 13 to 16 August 2000 (contour map is 0000 UTC surface analysis; shaded map is 0000 UTC 500 hPa analysis) and average concentration of O_3 ($\mu g\ m^{-3}$) in the lower troposphere of southwestern Europe and the NWMB during the episode of 13–16 August 2000 as simulated by ECHAM5/MESSy.

Dudhia simple ice moisture scheme, the cloud-radiation scheme, and the five-layer soil model. Initialization and boundary conditions for the mesoscale model were introduced with analysis data of the European Centre of Medium-range Weather Forecasts global model (ECMWF). Data were available at a 1° resolution (about 100 km at the NWMB latitude) at the standard pressure levels for every 6 hours.

[14] The high-resolution (1 hour and 1 km^2) EMICAT2000 emission model [*Parra et al.*, 2006] has been applied to the model domain. This model includes the emissions from vegetation, road traffic, industries and emissions by fossil fuel consumption, domestic/commercial and solvent use. Biogenic emissions were estimated using a methodology that takes into account local vegetation data (land use distribution and biomass factors) and meteorological conditions (surface air temperature and solar radiation) together with emission factors for the native Mediterranean vegetation [*Parra et al.*, 2004]. Road traffic sources include the hot exhaust, cold exhaust and evaporative emissions using the methodology and emission factors of the European model EMEP/CORINAIR – COPERTIII [*Ntziachristos and Samaras*, 2000] as a basis, and distinguishing between the weekdays and weekends vehicle park composition [*Jiménez et al.*, 2005a]. Industrial emissions include records of some chimneys connected to the emission control net (XEAC) of the Environmental Department of the Catalonia Government (Spain), and the estimated emissions from power stations (conventional and cogeneration units), cement factories, refineries, olefins plants, chemical industries and incinerators.

[15] The chemical transport model used to compute the concentrations of photochemical pollutants was Models-3/CMAQ [*Byun and Ching*, 1999]. The initial and boundary conditions were derived from a one-way nested simulation covering a domain of 1392 × 1104 km^2 centered in the Iberian Peninsula, that used EMEP emissions corresponding to year 2000 (http://www.emep.int). A 48-hour spin-up was performed to minimize the effects of initial conditions [*Berge et al.*, 2001]. The chemical mechanism selected for the simulations (based on the work by *Jiménez et al.* [2003b]) was CBM-IV [*Gery et al.*, 1989], including aerosols and heterogeneous chemistry. NO_x and VOC specification of EMICAT2000 emissions, as required by CBM-IV, are detailed by *Parra et al.* [2006]. The algorithm chosen for the resolution of tropospheric chemistry was the Modified Euler Backward Iterative (MEBI) method [*Huang and Chang*, 2001]. The horizontal resolution considered was 2 km, and 16-sigma vertical layers cover the troposphere.

2.3. Back Trajectory Analysis

[16] To analyze the origin of air masses over the NWMB, back trajectory analysis by means of the HYSPLIT trajectory model [*Draxler and Hess*, 1998] was performed for the episode studied (13–16 August 2000) using MM5 meteorological model output. Simulations were performed in four nested domains, which essentially covered Europe (domain 1, D1), the Iberian Peninsula (domain 2, D2), the northeastern Iberian Peninsula (domain 3, D3) and the Catalonia area (domain 4, D4). D1 is formed by 35 × 50 grid points in the horizontal with 72-km grid point spacing; D2, 61 × 49 24-km cells; D3, 93 × 93 6-km cells; and D4, 151 × 151 2-km cells.

3. Evaluation of ECHAM5/MESSy and MM5-EMICAT2000-CMAQ

[17] Air quality station hourly data, averaged over the domain of study, were used to evaluate the performance of both ECHAM5/MESSy and MM5-EMICAT2000-CMAQ predicting ground-level O_3, CO and NO_x over the episode of 13–16 August 2000. Hourly measurements of ambient pollutants were provided by 48 air quality surface stations (XVPCA) in northeastern Spain, which are part of the Environmental Department of the Catalonia Government (Spain). The European Directive 2002/3/EC related with O_3 in ambient air assumes an uncertainty of 50% for the air quality objective for modeling assessment methods. This uncertainty is defined as the maximum error of the measured and calculated concentration levels. In addition, the US Environmental Protection Agency has recently developed new guidelines [*U.S. Environmental Protection Agency* (*U.S. EPA*), 2005] for a minimum set of statistical measures to be used for these evaluations in regions where monitoring data are sufficiently dense. These guidelines indicate that it is inappropriate to establish a rigid criterion for model acceptance or rejection (i.e., no pass/fail test). However, in the EPA guide for the 1-hour ozone attainment demonstrations [*U.S. EPA*, 1991], several statistical goals were identified for operational model performance. These goals were identified by assessing past modeling applications of ozone models and determining common ranges of bias, error, and accuracy. These statistical measures considered are the mean normalized bias error (MNBE); the mean normalized gross error for concentrations above a prescribed threshold (MNGE), and the unpaired peak prediction accuracy (UPA).

[18] Table 1 summarizes the results of the statistical analysis. Although there is no criterion for a "satisfactory" model performance, *U.S. EPA* [1991, 2005] suggested values of ±10–15% for MNBE, ±15–20% for the UPA and 30–35% for the MNGE to be met by modeling simulations of O_3, to be considered for regulatory applications. In addition, results of an evaluation of ECHAM5/MESSy and MM5-EMICAT2000-CMAQ for the locations of several air quality stations is shown in Figure 3 for urban (Barcelona and Vic), industrial (Alcover and Mataró) and background (Agullana and Begur) environments. The performance objective in the Directive 2002/3/EC (deviation of 50% for the 1 hour averages during daytime) is achieved for the entire period of study for both ECHAM5/MESSy and MM5-EMICAT2000-CMAQ. The modeled episode peak concentration (189 $\mu g\ m^{-3}$) is well captured by both models (163 $\mu g\ m^{-3}$ and 188 $\mu g\ m^{-3}$ in the case of ECHAM5/MESSy and MM5-EMICAT2000-CMAQ, respectively). The unpaired peak accuracy is negative during the simulated episode when considering ECHAM5/MESSy outputs; this underprediction ranges from −15.9% to −4.7%. UPA is overestimated by MM5-EMICAT2000-CMAQ for the first and last day of simulations (14.4% and 5.2%, respectively) and underestimated for the central days of the episode (−3.8% and −11.7%).

[19] Despite considerably different approaches and resolutions both models meet the objective of ±20% set by US

Table 1. Criteria to Be Met by Photochemical Models and the Results Obtained for the Northwestern Mediterranean Basin Using ECHAM5/MESSy and MM5-EMICAT2000-CMAQ for the Episode of 13–16 August 2000

	Ozone (Observations)								
	13 Aug 2000			14 Aug 2000		15 Aug 2000		16 Aug 2000	
Observed Peak, $\mu g\ m^{-3}$	157			177		189		171	
	Ozone (Model)								
		13 Aug 2000		14 Aug 2000		15 Aug 2000		16 Aug 2000	
	EPA Goal	ECHAM5	CMAQ	ECHAM5	CMAQ	ECHAM5	CMAQ	ECHAM5	CMAQ
Modeled peak, $\mu g\ m^{-3}$		137	189	151	170	159	167	163	180
UPA, %	<±20	−12.7	14.4	−14.7	−3.8	−15.9	−11.7	−4.7	5.2
MNBE, %	<±15	12.4	−2.1	13.1	−11.0	14.3	−10.3	15.8	−5.6
MNGE, %	<35	19.2	16.8	27.6	19.8	28.6	21.7	31.3	26.7

EPA for UPA; hence they are considered to be accurate tools to forecast the O_3 peak levels. The O_3 bias of ECHAM5/MESSy is positive on each day of the simulation, progressively increasing from 12.4% until 15.8% on the last day of the episode. This positive bias may be due to an excessive accumulation of O_3 during this low-pressure gradient situation or an underestimation of the drainage flows over the region. On the other hand, MM5-EMICAT2000-CMAQ underpredicts average O_3 concentrations over the MNBE, with negative biases of −2.1% for the first day of simulation up to −11.0% for 14 August 2000. This overall negative bias may suggest that the O_3 production chemistry in MM5-EMICAT2000-CMAQ may not be sufficiently efficient. US EPA goals of ±15% are achieved by both MM5-EMICAT2000-CMAQ and ECHAM5/MESSy; although the latter produces higher positive biases indicating an overestimation of mean values. The MNGE increases from 13 until 16 August 2000 in simulations with both models (19% to 31% for ECHAM5/MESSy and 17% to 27% for MM5-EMICAT2000-CMAQ). This increment may be due to deviations in meteorological predictions that grow with time in the simulation [*Jiménez et al.*, 2005a]. However, the MNGE derived from the results achieve the EPA goals for a discrete evaluation on all episode days for both models (<35%).

[20] Table 2 presents the results of the evaluation of ECHAM5/MESSy and MM5-EMICAT2000-CMAQ with different statistical parameters for O_3, CO and nitrogen oxides (NO_x). Evaluation against 1649 measurements is performed in the case of O_3. Results for O_3 show a correlation of 0.62 and 0.74 for ECHAM5/MESSy and MM5-EMICAT2000-CMAQ, respectively. Simulations for CO and NO_x tend to show larger biases and errors than the corresponding statistics of O_3 for the same simulation. As noted by *Russell and Dennis* [2000], current air quality models have a pervasive tendency toward the underprediction of O_3 precursors. In the case of CO, the correlation coefficient between the observed and predicted CO concentrations for the 907 observation values during this episode is 0.34 for ECHAM5/MESSy and 0.57 for CMAQ, and hence correlating worse than O_3 in the domain of study. The mean bias is $-104.2\ \mu g\ m^{-3}$ and $-102.3\ \mu g\ m^{-3}$, for ECHAM5/MESSy and MM5-EMICAT2000-CMAQ, respectively. In the case of NO_x, ECHAM5/MESSy and MM5-EMICAT2000-CMAQ have normalized biases of −20% and −9%, respectively. The simulation with the coarser grid (ECHAM5/MESSy) underestimates maximum O_3, CO and NO_x levels relative to the fine grid of MM5-EMICAT2000-CMAQ, considering that the resolution strongly influences the formation and loss processes of pollutants, (especially photochemistry and vertical transport). Hence the average volume defined by the model horizontal grid spacing must be sufficiently small to allow the air quality to be reproduced accurately [*Jang et al.*, 1995; *Jiménez et al.*, 2005b]. It appears that a finer grid is important for addressing O_3 processes in urban and industrial areas, whereas for rural areas larger grids may be allowed, for example, to capture the nonlinearity of the O_3 chemical formation as a function of precursor concentrations.

[21] The vertical O_3 profile evaluation of air quality models is not always straightforward since measurements are often lacking. Measurements by Lidar may alleviate this problem by providing vertical profiles showing the stratification of pollutants over a particular location, assumed to be representative of the region, or at least of a vertical column of the model [*Duclau et al.*, 2002]. For the episode selected (13–16 August 2000), *Pérez et al.* [2004] performed measurements using an elastic-backscatter Lidar on 14 August 2000, over the city of Barcelona. In this section we compare the simulation results with the profiles generated by the Lidar campaign.

[22] The vertical profiles obtained over the city of Barcelona (41.361°N–2.181°E) with the global model ECHAM5/MESSy and the regional modeling system MM5-EMICAT2000-CMAQ are shown in Figure 4. The results indicate that the profiles are comparable; and both models simulate a realistic O_3 gradient between the boundary layer and the free troposphere, whereby the differences between both models are mostly related to the representation of the planetary boundary layer.

[23] The vertical resolution of MM5-EMICAT2000-CMAQ is finer in the lower troposphere and the model results show a more detailed layering of pollutants within the lower kilometer. ECHAM5/MESSy calculates O_3 and CO concentrations between 500 m and 1000 m that are slightly higher than the MM5-EMICAT2000-CMAQ model. A relatively coarse vertical resolution of the lower troposphere leads to artificial vertical exchange between the boundary layer and the free troposphere, which enhances NO_x venting from the planetary boundary layer [*Wang et al.*, 1998] so that free tropospheric O_3 formation may be overestimated in the models with coarse resolution.

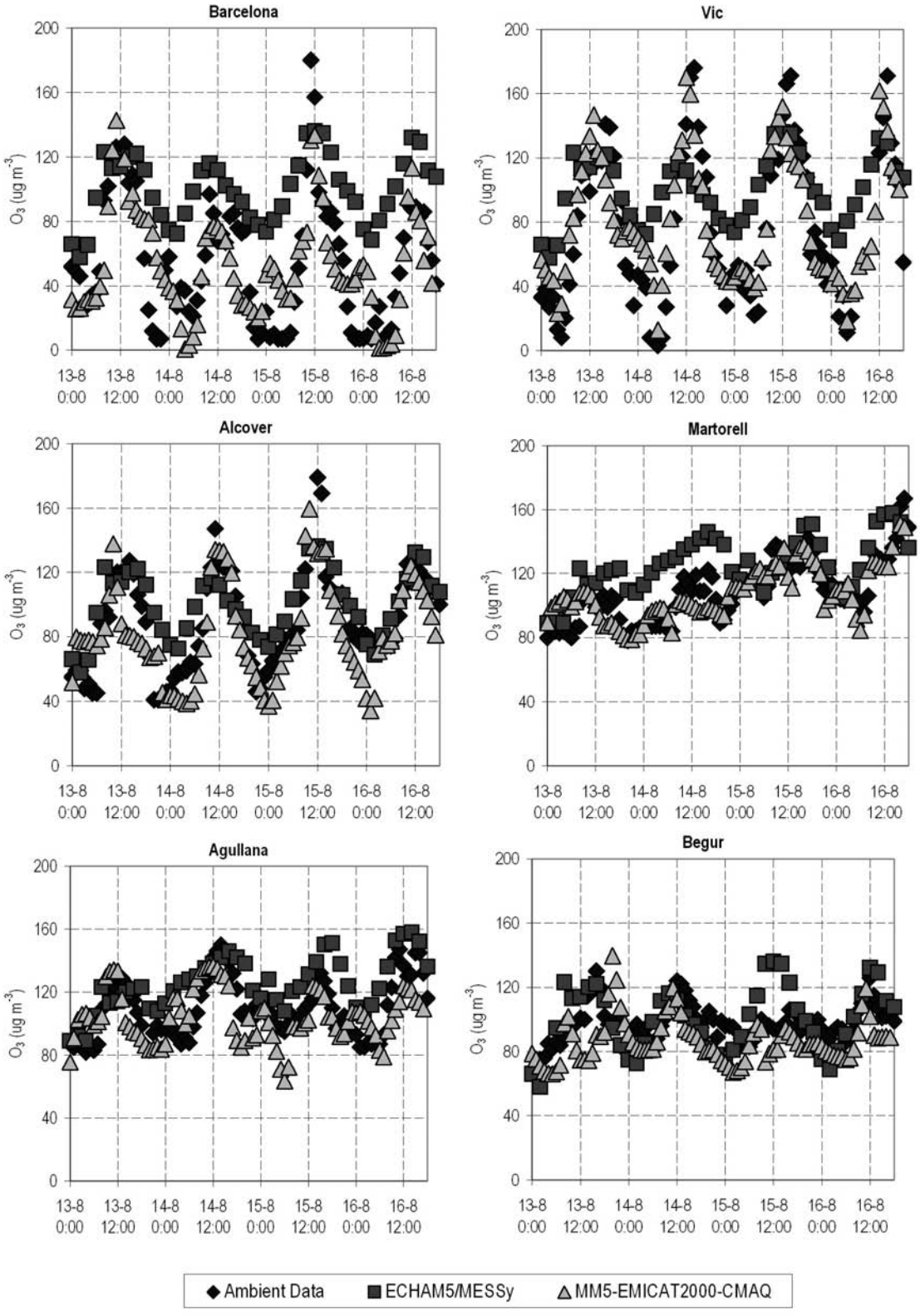

Figure 3. Ozone evaluation of ECHAM5/MESSy (squares) and CMAQ (triangles) with several air quality station data (diamonds) in the domain of the NWMB: urban (Barcelona and Vic), industrial (Alcover and Mataró) and background (Agullana and Begur).

Table 2. Results of the Evaluation of O_3, CO and NO_x With the ECHAM5/MESSy and MM5-EMICAT2000-CMAQ Models Against Data From 48 Air Quality Stations Located in the Northwestern Mediterranean Basin[a]

	Observations	ECHAM5	CMAQ
	Ozone (O_3)		
Mean, μg m^{-3}	63.7	88.2	64.7
SD, μg m^{-3}	37.4	16.7	31.5
CV, %	58.7	18.9	48.6
Max, μg m^{-3}	189.0	163.0	188.0
Min, μg m^{-3}	1.0	49.4	0.1
n		1649	1649
R		0.62	0.74
MB, μg m^{-3}		20.0	0.5
MNBE, %		46.8	37.9
MFB, %		21.1	5.6
MAGE, μg m^{-3}		25.9	9.8
MNGE, %		70.9	64.1
NME, %		42.2	30.8
NMB, %		28.0	1.7
RMSE, μg m^{-3}		37.2	12.7
	Carbon Monoxide (CO)		
Mean, μg m^{-3}	908.1	788.4	826.5
SD, μg m^{-3}	325.0	265.3	287.2
CV, %	35.8	31.6	34.8
Max, μg m^{-3}	2000.0	1610.0	1832.3
Min, μg m^{-3}	300.0	475.0	271.0
n		907	907
R		0.34	0.57
MB, μg m^{-3}		−104.2	−102.3
MNBE, %		−3.1	−8.0
MFB, %		−12.2	−13.1
MAGE, μg m^{-3}		311.6	188.4
MNGE, %		35.1	18.6
NME, %		35.9	35.1
NMB, %		−13.2	−22.8
RMSE, μg m^{-3}		285.8	242.9
	Nitrogen Oxides (NO_x)		
Mean, μg m^{-3}	59.5	66.6	54.0
SD, μg m^{-3}	45.5	43.9	51.7
CV, %	76.4	66.0	95.6
Max, μg m^{-3}	279.3	190.0	283.0
Min, μg m^{-3}	2.8	15.0	1.2
n		907	907
R		0.56	0.75
MB, μg m^{-3}		−14.5	−5.5
MNBE, %		−10.5	−6.1
MFB, %		−26.3	−23.8
MAGE, μg m^{-3}		31.9	26.3
MNGE, %		43.0	62.7
NME, %		44.3	44.4
NMB, %		−20.2	−9.2
RMSE, μg m^{-3}		41.1	35.4

[a]SD, standard deviation; CV, coefficient of variation; Max, maximum; Min, minimum; n, number of observations; R, regression coefficient; MB, mean bias; MNBE, mean normalized bias error; MFB, mean fractional bias; MAGE, mean absolute gross error; MNGE, mean normalized gross error; NME, normalized mean error; NMB, normalized mean bias; and RMSE, root mean square error.

[24] The Lidar profiles show that multiple layers occur above the mixing layer at 700–800 m between 1400 UTC and 1500 UTC [*Pérez et al.*, 2004]. Simulations with MM5-EMICAT2000-CMAQ capture this feature (both for O_3 and CO); this layer is associated with local recirculations over coastal and precoastal mountain ranges. However, the coarser ECHAM5/MESSy model (referring to both vertical and horizontal resolution) is not able to capture this feature of the flow (Figure 4). According to *Roelofs et al.* [2003], the horizontal and vertical resolutions included in ECHAM5/MESSy model may be too coarse to accurately represent some of the relevant boundary conditions in detail (e.g., height and stability of the land-sea breeze circulations). The Lidar measurements indicate another layer between 1600 and 2300 m, being reproduced both by the regional and the global models, especially in the case of photochemical O_3, with concentrations of 105 μg m^{-3}. This layer is formed by the return flow of the breeze in combination with the flows along coastal and precoastal mountain ranges. It is remarkable that this is also observed in the CO simulation results, depicting a layer with relatively low concentrations (260 μg m^{-3}) though rich in O_3 and aerosols. Finally, the Lidar detected a layer with a peninsular-scale origin at an altitude up to 3500 m. Simulations with both models indicate a layer with a relatively high CO content (>300 μg m^{-3}) between 2600 and 4000 m. In the simulated vertical profile of O_3 this layer is difficult to distinguish from the layer below (1600–2300 m) and other possible layers above, possibly associated with excessive exchange between these layers.

4. Source Attribution to Tropospheric Ozone and Carbon Monoxide

[25] In this section we discuss the contributions of main atmospheric processes to the levels of pollutants at the surface and their budget in the overhead tropospheric column. Processes considered include (1) emissions and photochemistry, (2) convective transport, (3) advective transport, (4) dry and wet deposition, and (5) stratosphere-troposphere exchange. Note that it did not rain during the period considered, so that category 4 is limited to dry deposition.

[26] The methods for performing the O_3 and CO budget follow the work by *O'Connor et al.* [2004]. The net photochemical term of the ozone budget was derived by integrating the difference in the tropospheric ozone burden before and after the chemistry calculations in ECHAM5/MESSy through the time period of 13–16 August 2000. The stratospheric input was calculated in the same way, although in this case, the difference used was that of the ozone burden before and after the call to the transport scheme. This was considered an appropriate method to calculate STE because the model's advective mass fluxes are highly variable and it was found that the calculation of the stratospheric source using these fluxes was very sensitive to the sampling frequency and the time period considered [*O'Connor et al.*, 2004]. For the dry deposition and wet deposition loss term, the ozone burden in the bottom layer was calculated every chemical time step. In this way, the integrated effect of deposition could be evaluated.

[27] Table 3 shows the model calculated contributions of these five categories of processes to ground-level maximum concentrations of O_3 and CO estimated by ECHAM5/MESSy for the episode of 13–16 August 2000 within the NWMB. This process attribution indicates that the occurrence of high O_3 concentrations results from a large difference between high local chemical production and the minor removal rates by transport and deposition processes. The O_3 accumulation by chemical production during the day strongly exceeds vertical convection and dry deposition removal rates,

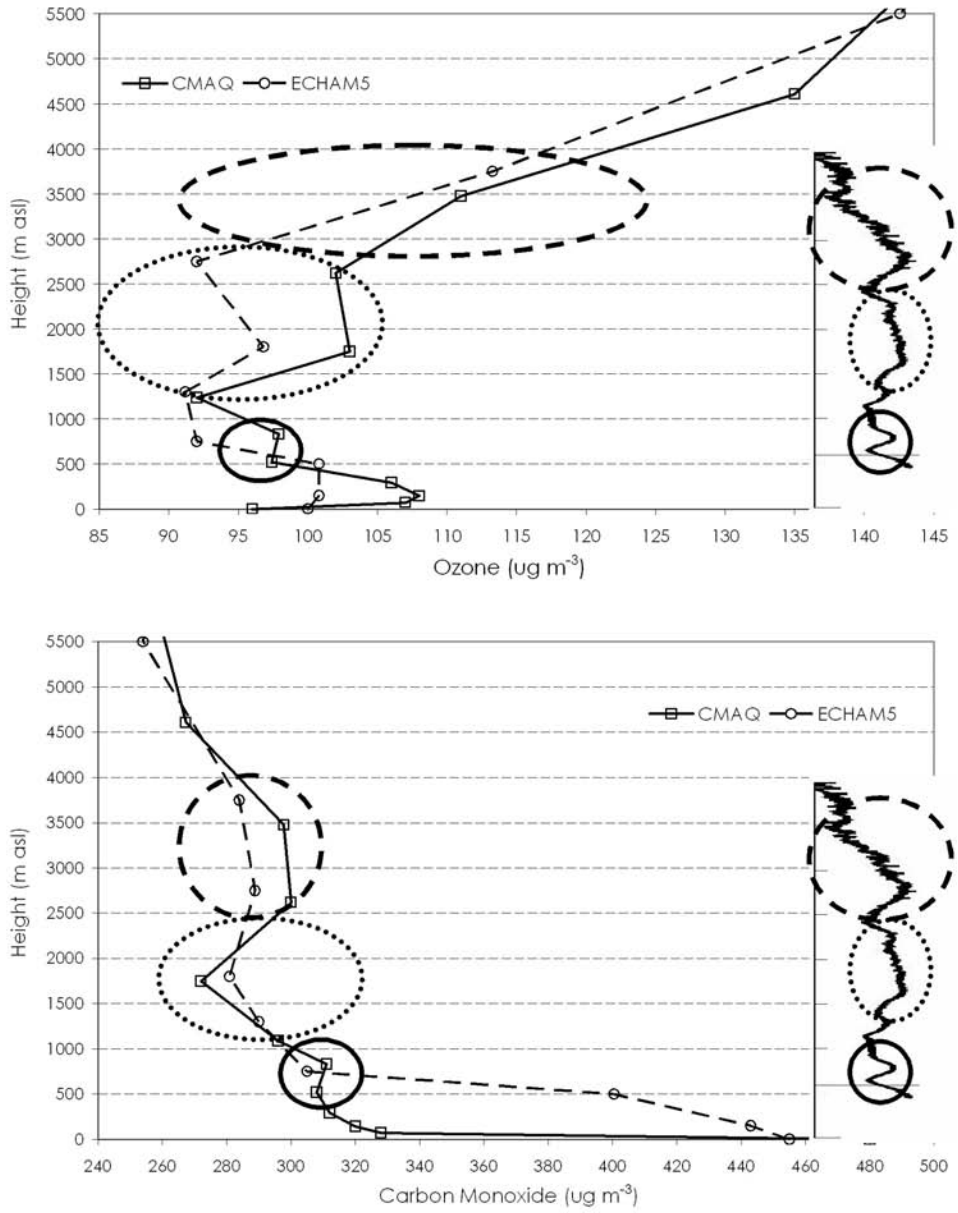

Figure 4. Layering of pollutants over the city of Barcelona, for (top) O_3 and (bottom) CO, on 14 August 2000 at 1500 UTC. Multiple layers appear at 700–800 m (solid), 1600–2300 m (dotted) and 2600–4000 m (dashed). Results from CMAQ (solid, squares), ECHAM5/MESSy (dashed, circles) and lidar profiles (backscatter lidar, solid) are by *Pérez et al.* [2004].

Table 3. Contribution of Different Physicochemical Processes to Maximum Ozone and Carbon Monoxide Ground-Level Concentrations in the Northwestern Mediterranean Basin for the Episode of 13–16 August 2000 Estimated With ECHAM5/MESSy

	Ground-Level O_3		Ground-Level CO	
	Concentration Contribution, μg m^{-3}	Percentual Contribution, %	Concentration Contribution, μg m^{-3}	Percentual Contribution, %
Emissions and photochemistry	186.9	114.4	712.5	97.9
Convective transport	−7.7	−4.7	−29.5	−4.1
Advective transport	6.8	4.2	46.3	6.4
Dry and wet deposition	−26.1	−16.0	−1.4	−0.2
S-T exchange	3.6	2.2	0.0	0.0
Total	163.3	100.0	727.9	100.0

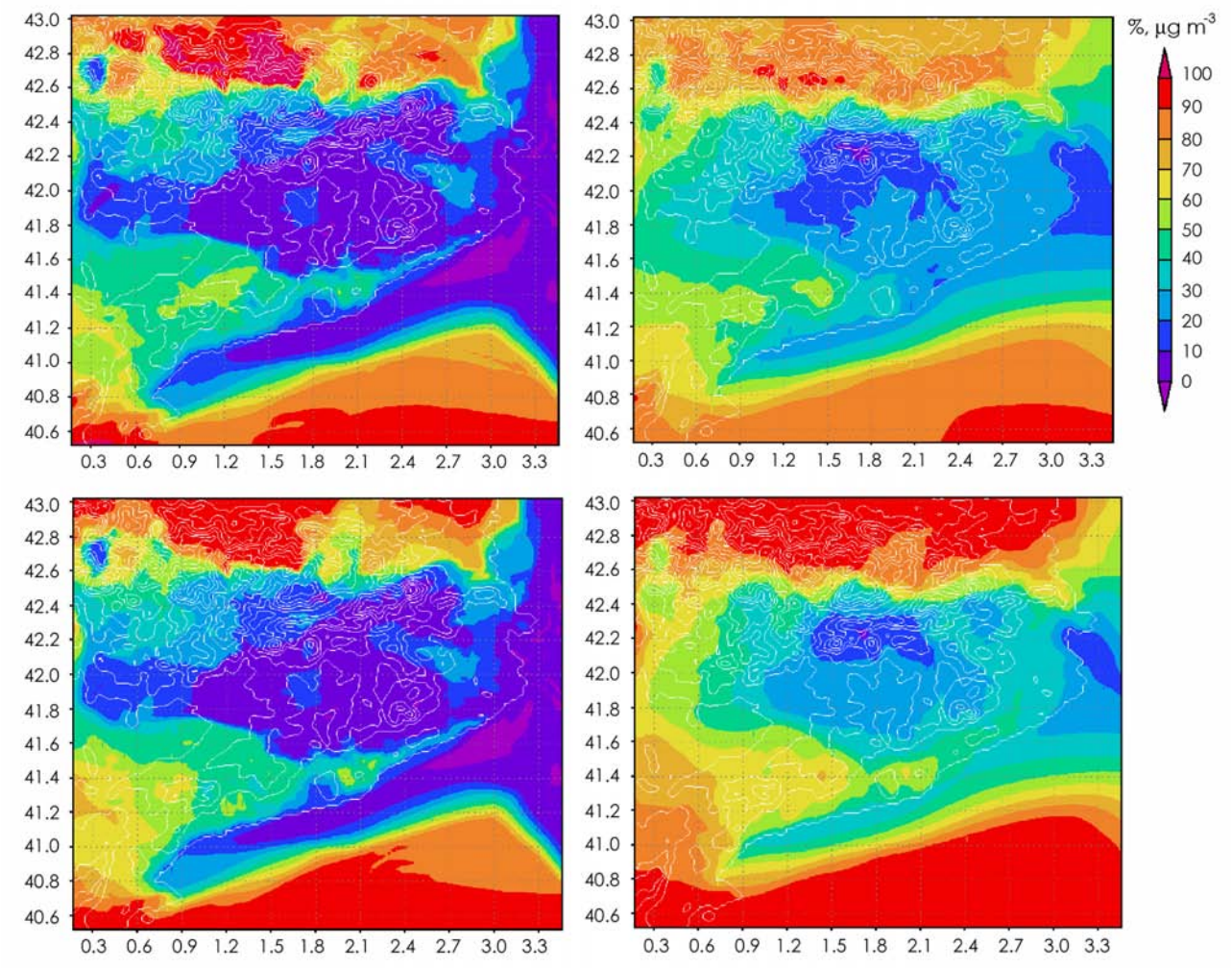

Figure 5. Difference in ozone between the base simulation and the simulation with "clean" boundaries in the PBL of the NWMB for 13–16 August 2000: (top left) difference in maximum 1 hour concentrations ($\mu g\ m^{-3}$), (bottom left) percentage difference for 1 hour peak values relative to the base simulation, (top right) difference in daytime average concentrations ($\mu g\ m^{-3}$) and (bottom right) percentage difference in mean concentrations relative to the base simulation.

leading to peak O_3 concentrations during the midafternoon, similar as inferred for other locations affected by photochemical air pollution [e.g., *Jian et al.*, 2003].

[28] In the area of study over the NWMB, the local emissions and net photochemical O_3 production dominate the maximum concentrations at the surface (186.9 $\mu g\ m^{-3}$ for O_3 and 712.5 $\mu g\ m^{-3}$ for CO), while dry deposition and convective vertical transport are the largest sinks in the case of O_3 ($-26.1\ \mu g\ m^{-3}$ and $-7.7\ \mu g\ m^{-3}$, respectively). For CO the contribution of deposition is only $-1.4\ \mu g\ m^{-3}$, and convective transport to the middle troposphere ($-29.5\ \mu g\ m^{-3}$) is the main removal process. The STE effect on O_3 at the surface is merely ~2% (3.6 $\mu g\ m^{-3}$ for O_3), while STE does not seem to affect CO. According to the ECHAM5/MESSy results, the advection term contributes only little to the maximum concentrations (6.8 $\mu g\ m^{-3}$ for O_3 and 46.3 $\mu g\ m^{-3}$ for CO), especially compared to the large local emission and chemical production. This is associated with the meteorological conditions during the episode (low pressure gradients within a weak anticyclone over the Mediterranean), which strongly limit transport processes in the area.

[29] To further account for the advective transport contribution to maximum 1-hourly peak O_3 levels by using MM5-EMICAT2000-CMAQ for the domain located in the NWMB, we conducted simulations with "clean" boundary conditions, i.e., zero concentrations at the domain boundaries. The results for the planetary boundary layer are shown for 1 hour maximum O_3 levels and daily mean O_3 concentrations in Figure 5.

[30] The modeled O_3 with MM5-EMICAT2000-CMAQ indicates that the most important influence of advective transport on O_3 (both for 1 hour maximum and average concentrations) occurs over the Mediterranean sea where O_3 precursor emissions are absent. Note that in these simulations ship traffic emissions have been neglected, so that these results represent an upper limit. A maximum simulated 1-hourly O_3 concentration occurs downwind the city Barcelona, at 41.842°N latitude and 2.305°E longitude (189.1 $\mu g\ m^{-3}$ in the base case, and 184.4 $\mu g\ m^{-3}$ in the

Table 4. Contributions of Physical-Chemical Processes to O_3 and CO Budgets in the Troposphere Over the Northwestern Mediterranean Basin for the Episode of 13–16 August 2000

	O_3 Budget		CO Budget	
	Mass Contribution, Gg	Percentual Contribution, %	Mass Contribution, Gg	Percentual Contribution, %
		PBL		
Emissions-photochemistry	48.1 Gg O_3	113.3%	132.6 Gg CO	98.5%
Convective transport	−1.5 Gg O_3	−3.5%	−5.1 Gg CO	−3.8%
Advective transport	1.3 Gg O_3	3.2%	7.4 Gg CO	5.5%
Dry and wet deposition	−6.5 Gg O_3	−15.4%	−0.3 Gg CO	−0.2%
S-T exchange	1.0 Gg O_3	2.4%	0.0 Gg CO	0.0%
Total	42.4 Gg O_3	100.0%	134.6 Gg CO	100.0%
		Surface-500 hPa (5,500 m)		
Emissions-photochemistry	141.7 Gg O_3	85.7%	281.9 Gg CO	83.2%
Convective transport	−0.4 Gg O_3	−0.3%	−2.3 Gg CO	−0.7%
Advective transport	20.9 Gg O_3	12.6%	59.5 Gg CO	17.6%
Dry and wet deposition	−6.5 Gg O_3	−3.9%	−0.3 Gg CO	−0.1%
S-T exchange	9.6 Gg O_3	5.8%	0.0 Gg CO	0.0%
Total	165.3 Gg O_3	100.0%	338.8 Gg CO	100.0%
		Surface-250 hPa (11,000 m)		
Emissions-photochemistry	192.1 Gg O_3	75.9%	306.4 Gg CO	82.9%
Convective transport	0.0 Gg O_3	0.0%	0.0 Gg CO	0.0%
Advective transport	22.7 Gg O_3	9.0%	63.5 Gg CO	17.2%
Dry and wet deposition	−6.5 Gg O_3	−2.6%	−0.3 Gg CO	−0.1%
S-T exchange	44.9 Gg O_3	17.7%	0.0 Gg CO	0.0%
Total	253.1 Gg O_3	100.0%	369.6 Gg CO	100.0%

case with clean boundary conditions). Therefore the contribution of advective transport to maximum O_3 levels is calculated to be 4.7 $\mu g\ m^{-3}$, which is only 2.5% of the overall maximum concentration. These results agree with those obtained by ECHAM5/MESSy (6.8 $\mu g\ m^{-3}$, being 4.2% of the 1 hour peak O_3 concentration).

[31] Table 4 presents an overview of the budget of tropospheric O_3 and CO for the NWMB episode of 13–16 August 2000. The budget terms are detailed for source and sink contributions, where possible. In addition, the mass balance for O_3 and CO is subdivided into different vertical zones of the troposphere, covering three altitude ranges from the surface to (1) the planetary boundary layer top; (2) the middle troposphere (500 hPa, i.e., 5500 m); and (3) the upper troposphere (250 hPa, i.e., 11,000 m). The percentages shown indicate the contribution of each process to the total tropospheric amount of O_3 or CO in the respective parts of the troposphere.

4.1. Emissions and Photochemistry

[32] The main emission sources in the domain of study are located at the coast, especially in the Barcelona urban area and the Tarragona industrial zone [*Parra et al.*, 2006]. Biogenic sources are also of great importance near the Mediterranean coast, representing 34% of the total annual VOCs emissions, especially since they contribute reactive compounds such as aldehydes and isoprene. This percentage increases during summertime because of the higher temperatures and solar radiation. The traffic emissions represent 58% of the emissions of NO_x and 36% of the VOCs, notably olefins and aromatic compounds. During summer, especially in August, the traffic emissions increase with the growing number of tourist vehicles during the peak holiday period. Main sources are located at the axis of roads parallel to the coast and in the regions of Barcelona and Tarragona.

[33] Industrial emissions represent 39% of the NO_x and 17% of the VOC emissions, and are located mainly in the industrial area of Tarragona. Further, the use of solvents represents 13% of VOCs emissions in the area [*Parra et al.*, 2006]. The source of precursors attributable to the industrial sector in the domain of study adds up to 41 Gg yr^{-1} of NO_x and 23 Gg yr^{-1} of VOCs. Annually, total emissions of O_3 precursors include 106.9 Gg yr^{-1} of NO_x (58% traffic emissions; 39% industrial emissions) and 99.3 Gg yr^{-1} of NMVOCs (34% biogenic emissions; 36% road traffic; 17% industrial emissions).

[34] Emissions of O_3 precursors during the episode of 13–16 August 2000 were 1.18 Gg for NO_x and 0.86 Gg for nonmethane VOCs. The ratio NMVOCs/NO_x, being 1.28 on the annual average, increases up to 1.73 for this episode of photochemical pollution because of the high temperatures and solar radiation, promoting, e.g., evaporative emissions from vehicles, storage of fuels and solvents, and by the vegetation.

[35] These strong biogenic and anthropogenic emissions fuel the formation of tropospheric O_3. This is not only the case at the surface, where the emissions and photochemistry account for 48.1 Gg O_3 and 136.2 Gg CO in the boundary layer during the episode considered. Up to an altitude of about 5500 m, this is still about 85% of the O_3 (141.7 Gg) and CO (281.9 Gg). For the domain of study this furthermore contributes more than 75% to the tropospheric O_3 column burden (192.1 Gg). This percentage is also very high for CO, i.e., more than 80% (Table 4).

4.2. Convective Transport

[36] Convective transport is a particularly efficient process for the fast removal of boundary layer air into the upper troposphere [*Hauf et al.*, 1995; *Ström et al.*, 1999; *Fischer et al.*, 2003]. As shown previously, strong thermally or mechanically driven convective cells appear over the

central plain of the NWMB, transporting polluted air masses to altitudes typically up to about 3.5 km. At this altitude the air masses are incorporated into the dominant synoptic flow and are transported toward the coast. Subsequently, the subsidence that compensates the Iberian thermal low carries the polluted air masses into the sea breeze cells in the lower troposphere. Similar mesoscale dynamical conditions have been described for the eastern Iberian coast at the Mediterranean Sea, based mainly on measurement campaigns [*Millán et al.*, 1992, 1997, 2000]. The consequent multilayer structures have also been experimentally verified over the city of Barcelona on the basis of Lidar measurements [*Baldasano et al.*, 1994; *Soriano et al.*, 2001; *Pérez et al.*, 2004].

[37] In the case of the NWMB, convection-driven processes export 1.5 Gg of O_3 out of the planetary boundary layer to middle and upper tropospheric altitudes, accounting for a decrease of 3.5% of the O_3 in the lower troposphere. In the case of CO, 5.1 Gg of lower troposphere CO is transported aloft (3.8%). The pollutants removed by vertical convective processes are mainly injected into the middle troposphere, between 3500–5500 m. The local transport loss of O_3 and CO from the middle to the upper troposphere is only 0.4 Gg O_3 and 2.3 Gg CO. If we consider the tropospheric column, convective transport is negligible since the vertical redistribution of O_3 and CO is not a major loss process on short timescales.

4.3. Advective Transport

[38] The contribution of advective transport within the planetary boundary layer is very limited, accounting only for 1.3 Gg O_3 (3.2%) and 7.4 Gg CO (5.5%). The low-pressure gradient over the Mediterranean basin limits advection during the episode of 13–16 August 2000. Local recirculation processes (local origin of air masses) dominate the transport of pollutants in the low troposphere.

[39] Most of the advective transport actually occurs in the middle troposphere, with a contribution of 19.6 Gg O_3 (compared to a total of 20.9 Gg O_3 in the domain from the surface up to the middle troposphere), representing 12.6% of the O_3 budget for this latitude region. In the case of CO, advective transport accounts for 17.6% of the budget up to 500 hPa. Advective transport contributions to the middle troposphere in our domain originate in the western part of the Iberian Peninsula and the North Atlantic area.

[40] In the upper troposphere only 1.8 Gg O_3 is advectively transported, whereas this contribution is 22.7 Gg O_3 in the entire tropospheric column (9.0%). For CO, the contribution of advection in the tropospheric column is 63.5 Gg (17.2%).

4.4. Dry and Wet Deposition

[41] The term dry deposition represents a complex sequence of atmospheric phenomena resulting in the removal of pollutants from the atmosphere to the Earth's surface. We have used the approach of *Ganzeveld et al.* [1998], which derives aerodynamic and stomatal resistances from parameters calculated by ECHAM5/MESSy. Wet deposition is parameterized according to *Roelofs and Lelieveld* [1995]. The dry deposition of O_3 in domain accounts for −6.5 Gg O_3 during the episode of 13–16 August 2000, which indicates that dry deposition removes 15.4% of the total amount of O_3 in the area of study. The contributions of dry deposition to the O_3 concentration in the columns up to the middle and upper troposphere are −3.9% and 2.6%, respectively. On the other hand, the dry deposition of CO is only −0.3 Gg CO (−0.2% of the total CO) and thus hardly contributes to the CO budget. The simulation results simulations also indicate a very limited contribution by wet deposition over the Pyrenees, being negligible for the considered summer episode over the NWMB.

4.5. Stratosphere-Troposphere Exchange (STE)

[42] In summer, the photochemical lifetime of O_3 in the lower troposphere is of the order of days, transport is less efficient and STE has a minimum in summer [*Lelieveld and Dentener*, 2000]. Therefore, for the episode of 13–16 August 2000, the STE has a minor contribution to O_3 in the PBL (1.0 Gg O_3, 2.4%). This percentage increases to 6% in the middle troposphere, where 8.6 Gg O_3 is of stratospheric origin (9.6 Gg due to STE). The model results indicate that the O_3 observed in the upper troposphere is more strongly associated with STE (18%), while the contribution by photochemistry in the troposphere decreases with altitude. In the upper troposphere, 35.3 Gg of the O_3 in our domain are transported by STE, adding to a total of 44.9 Gg O_3 for the entire troposphere.

5. Ozone Dynamics in the NWMB

5.1. Lower Troposphere: Local Recirculations

[43] In summer the Mediterranean region is located between the Azorean high and Asian monsoon low-pressure regimes. This quasi-permanent weather system causes north-northwesterly flows aloft over the Mediterranean. Although this flow is strongest and most persistent in August [*Lelieveld et al.*, 2002], during the NWMB episode of 13–16 August 2000, the Azorean anticyclone dominated the weather over the Iberian Peninsula, with locally very low pressure gradients. At the surface a high-pressure ridge of about 1020 hPa penetrated over the NWMB. Within the anticyclone subsidence contributed to the accumulation of air pollution.

[44] The backward trajectories ending in the boundary layer and the lower troposphere (Figure 6) point to a local origin of air masses associated with recirculation processes, common in the western Mediterranean basin during summer [e.g., *Millán et al.*, 1992, 1997; *Baldasano et al.*, 1994]. The back trajectories at ground level indicate a regional recirculation regime over the Mediterranean Sea, while back trajectories at 500 m are suggestive of transport from the Valencia-Castellón area, with a potential industrial influence. This pattern remains very similar up to an altitude of about 2.5 km. Therefore, during 13–16 August 2000, photochemical pollution accumulated in the NWMB, as mentioned above.

[45] Figures 7 and 8 show the diurnal O_3 patterns on 14 August 2000 calculated with the two models. During nighttime the entire eastern Iberian coast was affected by down-slope winds from the mountains and generally offshore breezes. The flow between the Pyrenees and the French Central Massif channeled the northwesterly wind to the Mediterranean Sea. Furthermore, the offshore flows drained the pollutants toward the coast through the river valleys. As

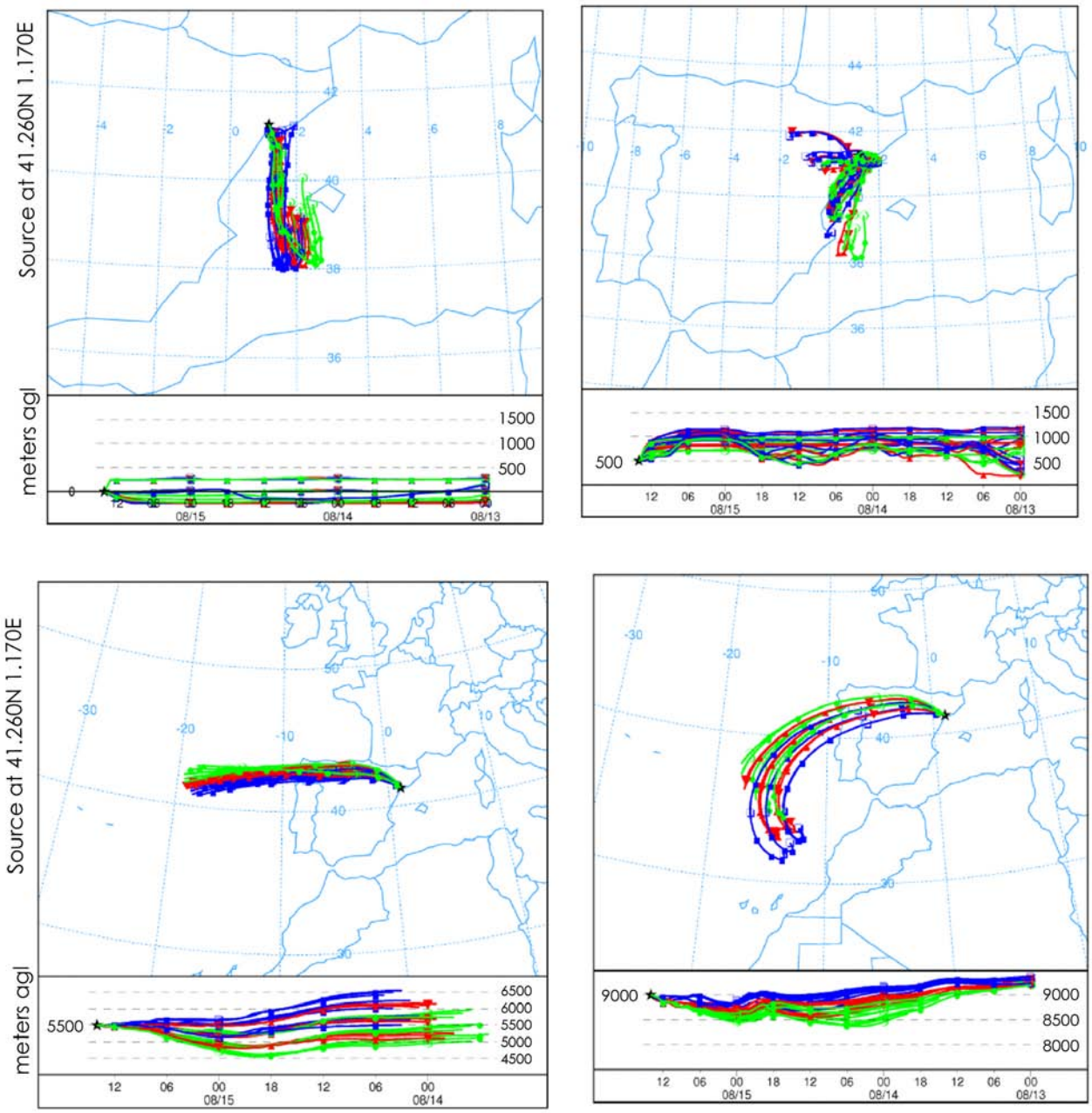

Figure 6. Ensemble 2.5-day back trajectories arriving at (top left) ground level, (top right) 500 m, (bottom left) middle troposphere and (bottom right) upper troposphere over the NWMB on 15 August 2000 at 1200 UTC.

the day advanced, a well-developed sea-breeze regime was established along the coast of the area with circulation cells reaching up to 2 km height, well above the PBL mixing height at about 800 m [*Sicard et al.*, 2006]. After 0800 UTC, onshore winds developed along the eastern Iberian coast, intensifying the anticyclonic circulation and deflecting the flow between the Pyrenees and the Central Massif toward the east.

[46] At noon, air pollution from the Barcelona area and the road axis along the coast was transported land inward following the breeze front (Figure 8), arriving, e.g., at Plana de Vic (70 km downwind of Barcelona), where the flow decelerates, allowing O_3 and its precursors to accumulate, thus exceeding the European Union threshold O_3 level of 180 $\mu g\ m^{-3}$. At the same time, in the southern part of the area of study (the industrial area of Tarragona), during the morning the katabatic winds weaken and a clear land-sea breeze develops, associated with anabatic and valley winds. The high O_3 concentrations in the southern NWMB are a consequence of the fact that the land-sea breeze is not sufficiently intense to overcome the littoral mountain range.

[47] Land inward of the NWMB, over the central plateau, the flow is influenced by the presence of the pre-Pyrenees and the northwesterly wind aloft, allowing recirculations

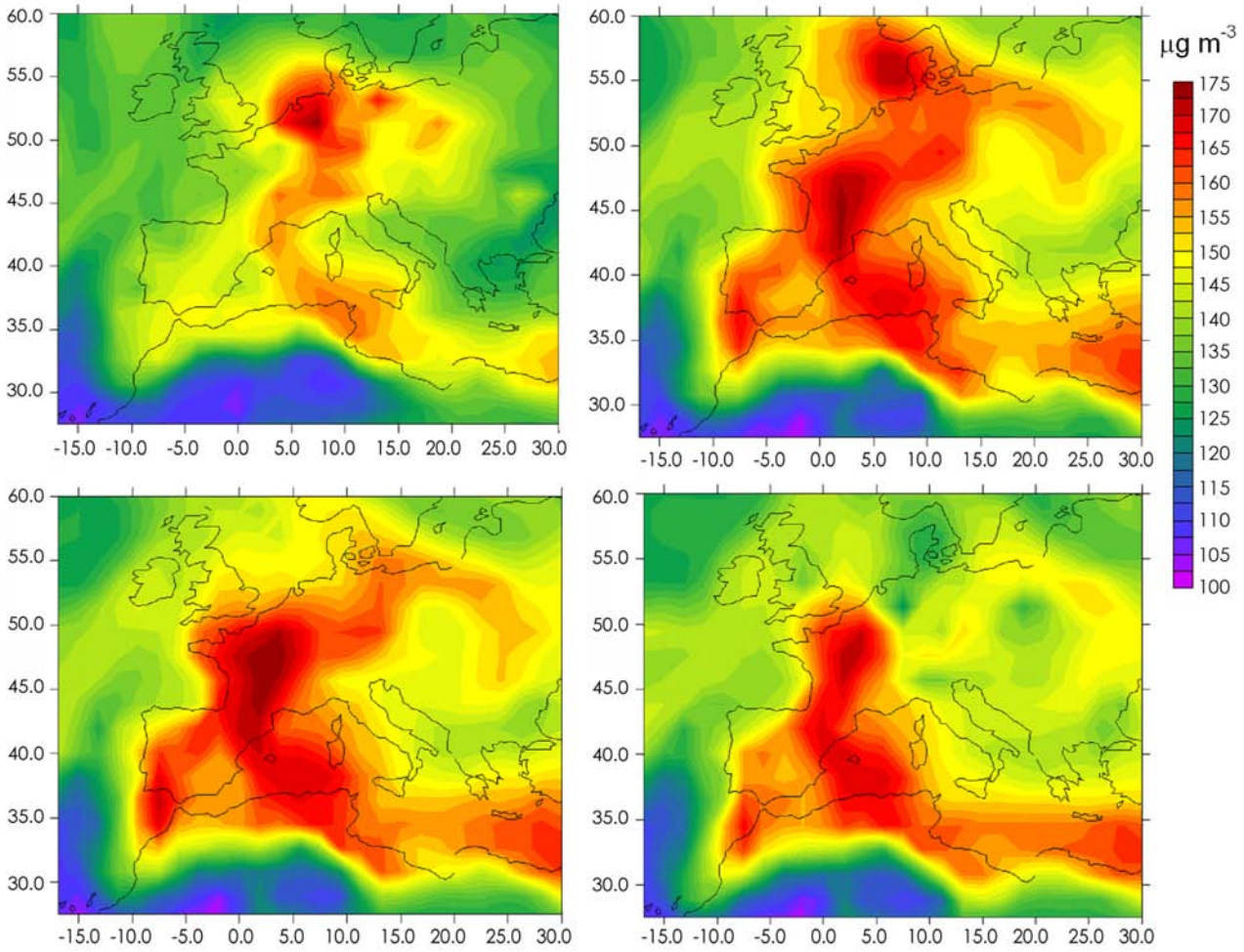

Figure 7. O_3 concentrations ($\mu g\ m^{-3}$) at ground level over southwestern Europe and the NWMB calculated with ECHAM5/MESSy for 14 August 2000 at (top left) 0600 UTC, (top right) 1200 UTC, (bottom left) 1600 UTC and (bottom right) 2000 UTC.

that also promote the accumulation of O_3. This pattern persists during the afternoon (Figure 8) although the breeze gains intensity and adds to the upslope winds, transporting pollutants over the prelittoral mountain ranges. Around 1900–2000 UTC, the photochemical activity ceases, the sea-breeze regime loses intensity and the coastal winds weaken. Inland, over the eastern part of the domain, strong southerly winds develop which dilute O_3. At night, land-inward winds calm with the development of a weak land breeze, with drainages in the valleys and katabatic winds. A larger-scale feature of the flow in the low troposphere is the wind canalization between the Pyrenees and the Central Massif, which introduces Atlantic air masses of northwesterly origin into the northeastern Iberian Peninsula region, as also concluded by *Gangoiti et al.* [2001]. The simulations with ECHAM5/MESSy and MM5-EMICAT2000-CMAQ indicate that the concentration of photochemical air pollution in these Atlantic air masses is relatively low.

[48] An important characteristic of the flow regime is that recirculations arise from the orographical forcing. The strength of the land-sea breeze and the complex orography along the eastern Iberian coast cause upward vertical injection and layering of the air pollution. As the sea breeze front advances inland reaching the mountain ranges, the orographically induced injection can occur at different altitudes, with a subsequent return flow toward the coast (Figure 9). Mechanical recirculation of air pollution can typically occur at Collserola Mountain (~500 m). At noon, the breeze usually reaches the first mountain chain, where it is reinforced by anabatic winds producing upward motions up to 1.5–2 km altitude.

5.2. Middle Troposphere: The Iberian Thermal Low (ITL)

[49] The intense surface heating promotes the development of the Iberian Thermal Low (ITL) over the central part of the Iberian Peninsula. The ITL system consists of at least three main cells [*Millán et al.*, 1996]: (1) The first is a coastal cell, which combines the sea breeze and up-slope winds and extends 80 to 100 km inland from the eastern Iberian coast; (2) the second cell is located over the central plateau; and (3) the third is a coastal cell symmetrical to that over the western Mediterranean basin which develops at the Atlantic coast. The ITL also developed during the episode of 13–16 August 2000, concurrent with the stagnant anticyclonic conditions.

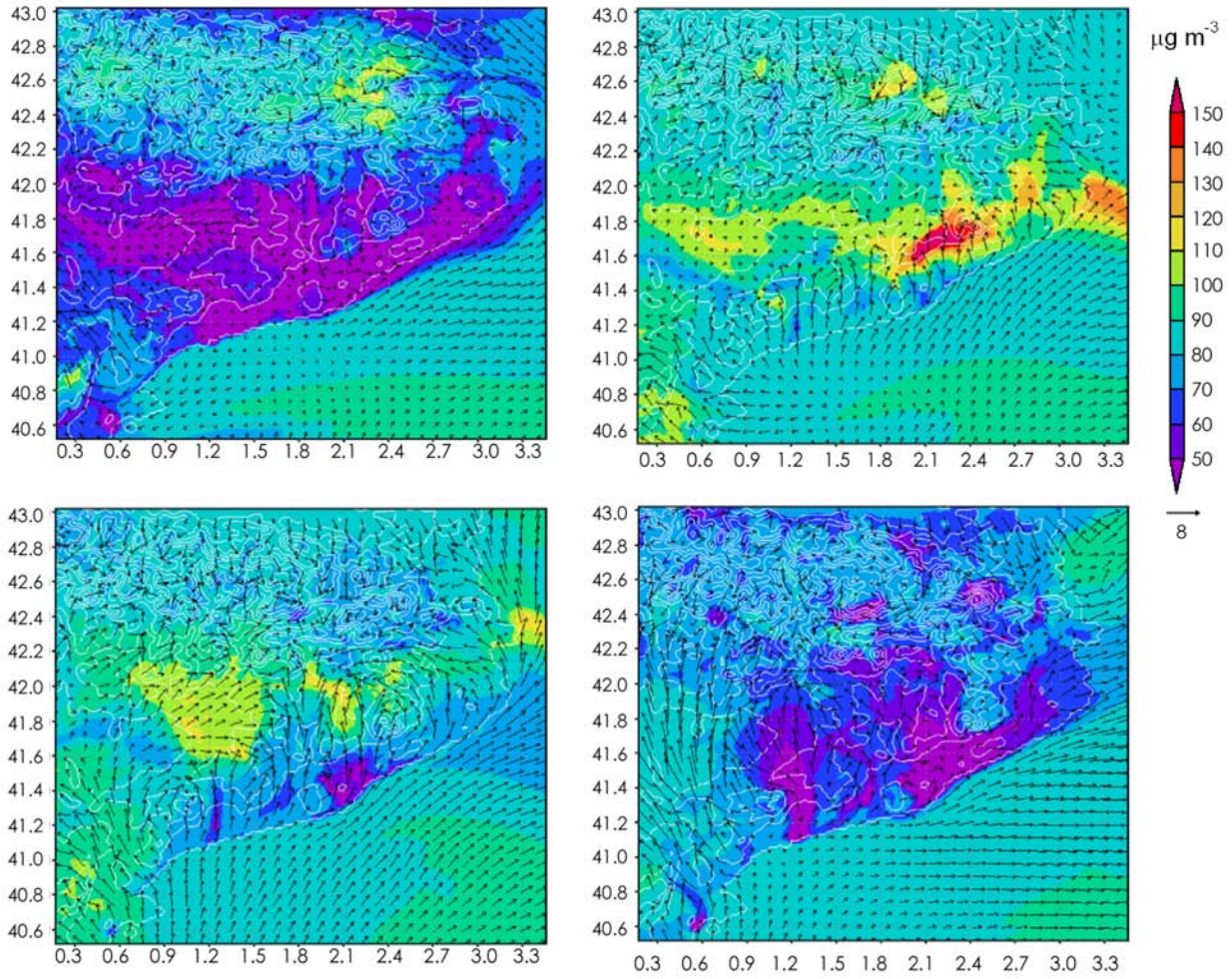

Figure 8. O_3 concentrations ($\mu g\ m^{-3}$) at ground level over southwestern Europe and the NWMB calculated with MM5-EMICAT2000-CMAQ for 14 August 2000 at (top left) 0600 UTC, (top right) 1200 UTC, (bottom left) 1600 UTC and (bottom right) 2000 UTC.

[50] This ITL at peninsular level forces the convergence of surface winds from the coastal areas toward the central plateau injecting polluted air masses into the middle troposphere. Once in this region, northwesterly winds transport pollutants within a stratified layer, clearly shown in the back trajectory analysis, indicating that air masses arriving in the NWMB have an Atlantic origin (Figure 6).

[51] Figure 10 indicates that this middle tropospheric air of Atlantic origin collects anthropogenic pollutants as the air masses flow over the central Iberian Plateau. The ECHAM5/MESSy simulations for 3.5 km altitude indicate that these air masses carry relatively much O_3 and precursor gases, injected by midlevel convective processes. In the middle troposphere medium-range transport toward the Mediterranean coast takes place, as indicated by the simulations with ECHAM5/MESSy and MM5-EMICAT2000-CMAQ. At 3–4 km altitude air masses with relatively high O_3 concentrations (>120 $\mu g\ m^{-3}$) are transported from the central plateau through the western boundary of the area of study at 0600 UTC. The anticyclonic subsidence contributes to the accumulation of air pollution over the littoral mountain ranges at least until 1800 UTC. Subsequently, the pollutants are transported toward the Mediterranean Sea where they further subside, which also contributes to the stabilization and layering of air pollution [*Gangoiti et al.*, 2001]. A fraction of these pollutants is incorporated into the sea breeze system during the following morning.

[52] On the other hand, some fraction is exported out of the domain of the NWMB by advective transport. These results agree with those by *Duncan and Bey* [2004], who present a study of the export pathways of pollution from Europe from 1987 to 1997, using a three-dimensional chemistry transport model. In summer, export occurs by both advection and convection; however, advective export of pollution predominates in the Mediterranean basin. Convective export seems to play a relatively minor role, despite of the similar overall conditions to those identified over other continents [*Wild and Akimoto*, 2001]. A conceptual representation of the dynamical processes influencing tropospheric O_3 is presented in Figure 11.

5.3. Upper Troposphere: Stratosphere-Troposphere Exchange (STE)

[53] The contribution of STE in tropospheric O_3 levels has been intensely studied previously [e.g., *Stohl and Trickl*, 1999; *Roelofs and Lelieveld*, 2000; *Lelieveld and Dentener*,

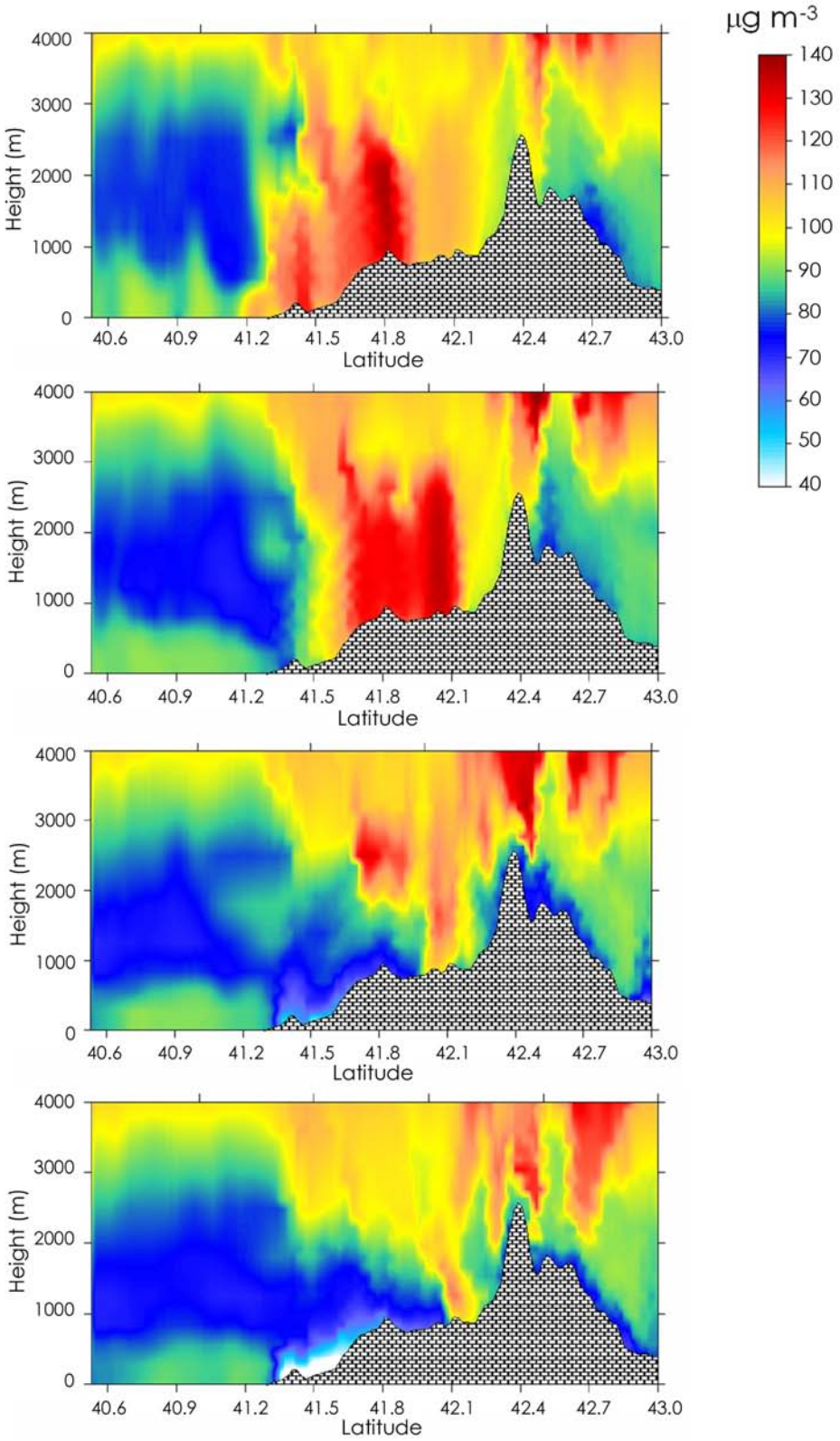

Figure 9. Recirculations over the northeastern Iberian Peninsula strongly influence O_3 (in $\mu g\ m^{-3}$) as calculated with MM5-EMICAT2000-CMAQ for 1200 UTC, 1400 UTC, 1800 UTC and 2000 UTC from top to bottom, respectively, for 14 August 2000.

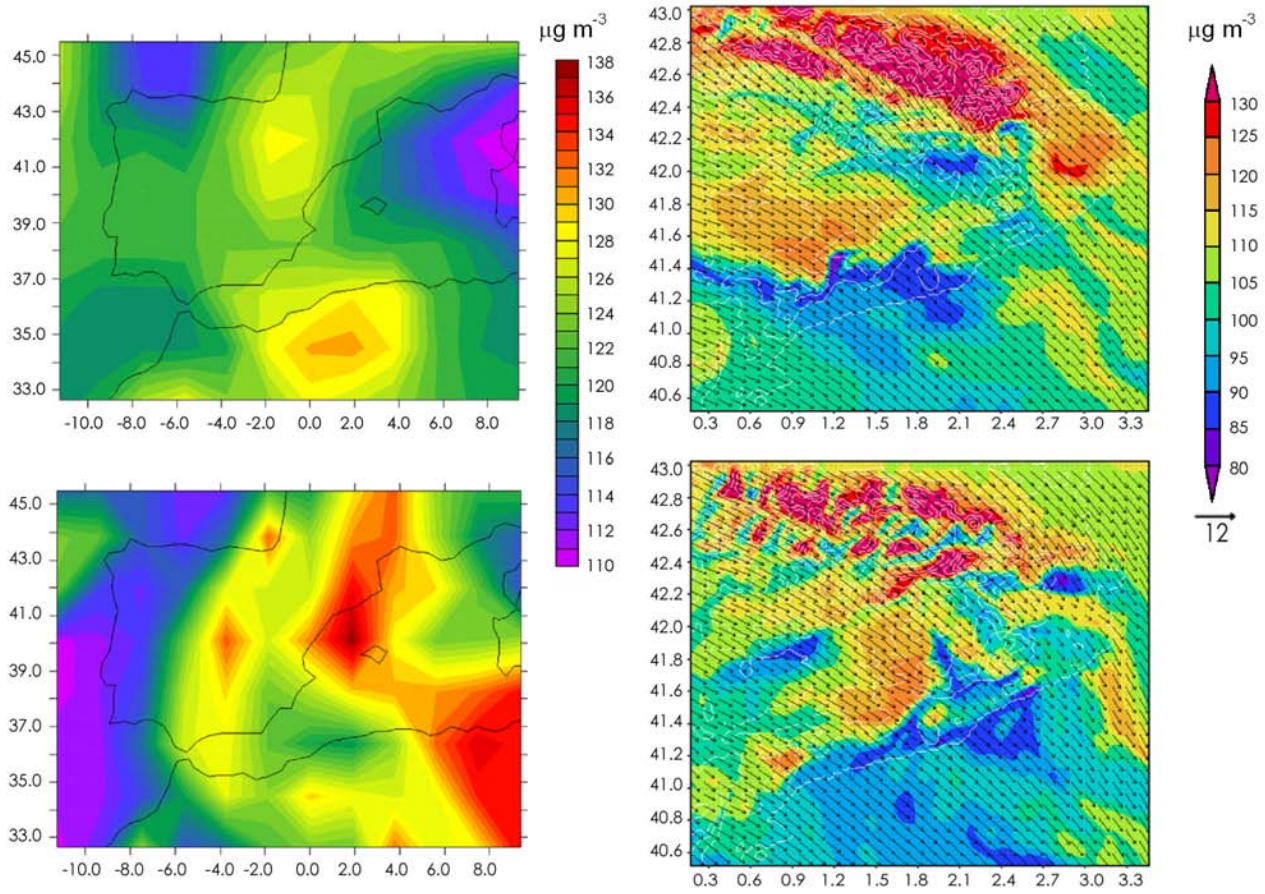

Figure 10. Ozone (in μg m^{-3}) at 3500 m, (top) 0600 UTC and (bottom) 1800 UTC on 14 August 2000 simulated (left) for southeastern Europe with ECHAM5/MESSy and (right) for the NWMB with MM5-EMICAT2000-CMAQ.

2000; *Traub et al.*, 2003]. The downward transport from the stratosphere to the troposphere is typically associated with the formation of tropopause folds [*Danielsen and Mohnen*, 1977], cutoff lows [*Bamber et al.*, 1984; *Wirth*, 1995a, 1995b] and streamers along the polar-front jet [*Appenzeller and Davies*, 1992]. Convective exchange processes furthermore enhance the downward transport of stratospheric air masses toward the middle and low troposphere [*Borchi and Marenco*, 2002; *Tulet et al.*, 2002].

[54] To determine the positions of the tropopause and the possible contributions of stratospheric ozone to O_3 levels in the NWMB, we have used the definition of potential vorticity (PV) proposed by *Reed* [1955]. *Hoerling et al.* [1991] point out that a value of 3.5 potential vorticity units (1 PVU = 10^{-6} m^2 s^{-1} K kg^{-1}) represents an optimal value for the definition of the tropopause outside the tropics; this has been the criterion used also by *Traub and Lelieveld* [2003]. In addition, the turbulence index (TI) by *Ellrod and Knapp* [1992] has been used to diagnose clear air turbulence (units are 10^{-7} s^{-2}).

[55] The meteorological analysis for the upper troposphere indicates relatively high pressures established over the African continent. In addition, an Atlantic depression progressed much further north, and over the Iberian Peninsula a weak zonal circulation dominated in the middle and upper troposphere, turning northwest over the Mediterranean coast. The ECHAM5/MESSy results show that a tongue-shaped area with PV values over 3.5 PVU extended along the eastern Mediterranean coast. A decreased tropopause height also occurred over the Sahara dessert and the northeastern Atlantic Ocean region. Coincident with the locations of high PV, an area with enhanced turbulence occurred over the eastern Mediterranean coast, the Sahara dessert and the northwestern Atlantic, with a TI index higher than 8. This turbulence, induced by upper level convergence near the tropopause and consequently strong wind shear, caused mixing of tropospheric and stratospheric air near the tropopause. High concentrations of O_3 associated with those tongue-shaped tropopause descends even reached the middle troposphere.

[56] Upper tropospheric back trajectories (about 9 km altitude) show that air masses were transported to the NWMB from Africa (Figure 6). Nevertheless, these air masses do not show strong vertical transport tendencies during the episode of 13–16 August 2000. Relatively high concentrations of tropospheric O_3 at about 300 hPa altitude over part of the Mediterranean area are explained by a strong stratospheric influence. However, owing to the stable stratification of the

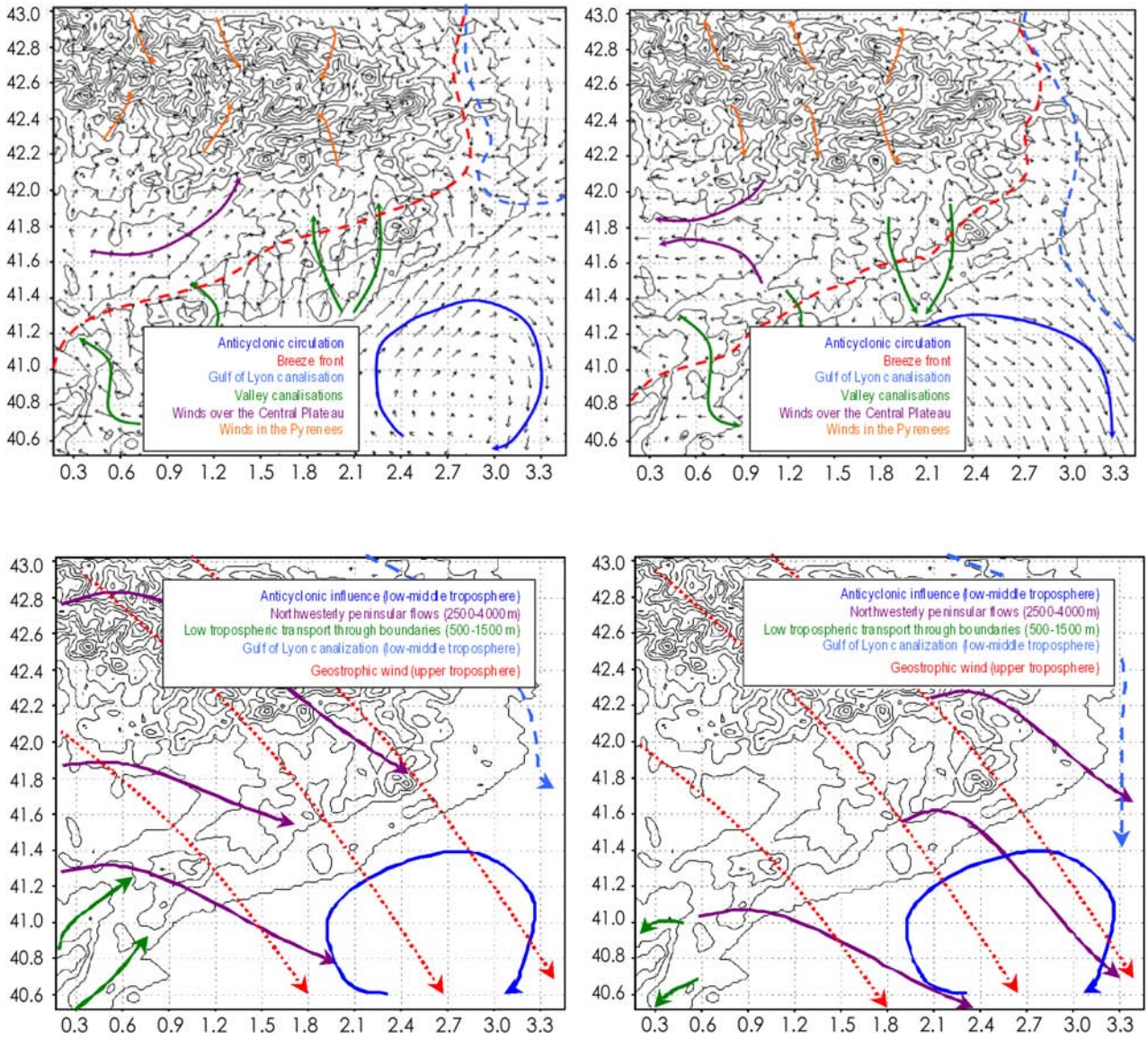

Figure 11. Conceptual representation of the flow regime during (left) daytime and (right) nighttime controlling (top) near-surface air pollution and (bottom) the atmospheric dynamics aloft over the NWMB during a typical summertime episode (13–16 August 2000).

Mediterranean troposphere these air masses have no direct influence on O_3 concentrations in the lower troposphere.

6. Conclusions

[57] The contributions of different physical-chemical processes to maximum concentrations of O_3 and CO at the surface in the area of the NWMB have been quantified using two models: ECHAM5/MESSy and MM5-EMICAT2000-CMAQ. This combination of models appears to provide a useful means to investigate the cycles and budgets of air pollutants at different resolutions, accounting for large-scale processes as well as local orographical and land-sea breeze circulations, which helps understanding the relative importance of coupled processes involved during air pollution episodes, in particular for this area. The complexity of the area of study requires the application of high-resolution (2 km and 1 hour) regional models to assess the coupled dynamics and the interaction of scales.

[58] The models were evaluated against ambient data from 48 air quality stations in the NWMB. The objective set in the Directive 2002/3/EC is achieved for the entire period of study for both ECHAM5/MESSy and MM5-EMICAT2000-CMAQ. Both models, despite considering different approaches and resolutions, met the objective of ±20% set by US EPA for prediction of the peak levels of this pollutant during the episode. However, the simulation with the coarser grid (ECHAM5/MESSy) underestimates maximum O_3, CO and NO_x levels with regards to the fine grid of MM5-EMICAT2000-CMAQ, since the grid resolution highly influences the formation and loss processes of pollutants (especially photochemistry and vertical transport). Vertical Lidar profiles obtained over the city of Barcelona (41.361°N–2.181°E) indicate that modeled profiles are sim-

ilar to measurements, capturing the layering of pollutants over the Mediterranean produced by recirculation processes. Both models produce a realistic O_3 gradient between the boundary layer and the free troposphere, and the differences between both models largely arise from the level of detail at which the planetary boundary layer is simulated.

[59] We have presented an overview of the NWMB budgets of tropospheric O_3 and CO for the episode of 13–16 August 2000, shown to be a representative case study. The budget terms for O_3 and CO distinguish different vertical parts of the troposphere, covering sections from the surface to (1) the top of the planetary boundary layer; (2) to the middle troposphere (500 hPa, ~5500 m); and (3) up to the upper troposphere (250 hPa, ~11000 m). Our analysis indicates that the occurrence of high O_3 concentrations mostly results from efficient local photochemical production, both in the planetary boundary layer and in the entire tropospheric column over the NWMB. The contribution of advective transport is limited, associated with the low-pressure gradient. The simulations with ECHAM5/MESSy and MM5-EMICAT2000-CMAQ consistently show that the contribution by advection to peak O_3 levels is only about 2.5–5%. The steady increase in photochemical production of O_3 during the day strongly exceeds the removal by convection and dry deposition, leading to peak O_3 concentrations during the midafternoon.

[60] With respect to the origin of the high levels of photochemical pollutants and their dynamics over the NWMB, the main processes that take place in the troposphere of the NWMB may be summarized as follows:

[61] 1. The episode of 13–16 August 2000, considered to analyze the processes over the NWMB, is characteristic for photochemical air pollution by O_3 during summertime, being related to a low-pressure gradient. The period was characterized by a weak synoptic forcing, so that mesoscale phenomena, induced by the particular geography of the region, were dominant. The air pollution in the lower troposphere had a local origin associated with recirculation processes, i.e., caused by the orographic forcing together with land-sea breeze circulations common in the NWMB.

[62] 2. During the episode a strong land-sea breeze regime established along the entire domain. Circulation cells up to 2 km height, substantially extending over the mixing height (800 m), developed in the morning hours. The strength of the sea breeze reinforced by the anabatic winds provoked by the complex orography of the eastern Iberian coast give rise to the vertical injection and layering of air pollutants. As the land-sea breeze front advanced inland, reaching the mountain ranges, orographical transport and mechanical recirculations of air pollutants occurred in the coastal mountains (~500 m). During the afternoon, the breeze reached the second mountainous chain, reinforced by anabatic winds, producing upward motions up to 1.5–2 km altitude. In the evening (2000 UTC) the photochemical activity ceased, the land-sea breeze regime lost intensity and coastal winds weakened, producing drainage of pollutants toward the coast through the river valleys. At night O_3 concentrations were further reduced as a consequence of titration by fresh NO emissions.

[63] 3. At an altitude of 0.5–1.5 km, air masses arriving in the NWMB had their origin near the southeastern Iberian coast. An O_3 reservoir layer at 1.5 km developed during the night over the Mediterranean Sea with O_3 concentrations in excess of 125 $\mu g\ m^{-3}$. The high-pressure area over the Mediterranean Sea was associated with anticyclonic circulation and therefore air pollutants were transported inland on the following day during the development of the land-sea breeze cycle.

[64] 4. The intense surface heating promoted the development of the ITL over the central Iberian Peninsula. It persisted with the stagnant meteorological conditions during the episode, and forced the convergence of surface winds from the coastal areas toward the central plateau over which convection transported polluted air masses into the middle troposphere. The northwesterly winds transported pollutants in a stratified layer at an altitude of 3.5 km toward the NWMB, where they further subsided and were incorporated into the land-sea breeze circulations.

[65] 5. In the upper troposphere air masses arriving in the NWMB originated from the tropopause region over of the Sahara dessert. They circulated over the Atlantic Ocean and the Iberian Peninsula with the northwesterlies aloft. The vicinity to the stratosphere and turbulent mixing processes explain the relatively high concentrations of O_3 at 300 hPa altitude. These high O_3 levels in the upper troposphere did not affect the lower troposphere.

[66] **Acknowledgments.** This work was developed under the research contract REN2003-09753-C02 of the Spanish Ministry of Science and Technology. We thank the Spanish Ministry of Education for the FPU doctoral fellowship granted to Pedro Jiménez. The authors gratefully acknowledge the MESSy team (Mainz, Germany) and the researchers at the Laboratory of Environmental Modeling (Barcelona, Spain) for helpful discussions and support. Air quality station data and information about industrial emissions were provided by the Environmental Department of the Catalonia Government (Spain).

References

Ancellet, G., and F. Ravetta (2005), Analysis and validation of ozone variability observed by lidar during the ESCOMPTE-2001 campaign, *Atmos. Res.*, *74*, 435–459.

Appenzeller, C., and H. Davies (1992), Structure of stratospheric intrusions into the troposphere, *Nature*, *358*, 570–572.

Baldasano, J. M., L. Cremades, and C. Soriano (1994), Circulation of air pollutants over the Barcelona geographical area in summer, in *Proceedings of Sixth European Symposium Physic-Chemical Behavior of Atmospheric Pollutants. Varese, Italy, 18–22 October, 1993*, *Rep. EUR 15609/1 EN*, pp. 474–479, Eur. Comm., Brussels.

Bamber, D., P. Healey, B. Jones, S. Penkett, A. Tuck, and G. Vaughan (1984), Vertical profiles of tropospheric gases: Chemical consequences of stratospheric intrusions, *Atmos. Environ.*, *18*, 1759–1766.

Barros, N., I. Toll, C. Soriano, P. Jiménez, C. Borrego, and J. M. Baldasano (2003), Urban photochemical pollution in the Iberian Peninsula: The Lisbon and Barcelona airsheds, *J. Air Waste Manage. Assoc.*, *53*, 347–359.

Berge, E., H.-C. Huang, J. Chang, and T.-H. Liu (2001), A study of the importance of initial conditions for photochemical oxidant modeling, *J. Geophys. Res.*, *106*(D1), 1346–1363.

Borchi, F., and A. Marenco (2002), Discrimination of air masses near the extratropical tropopause by multivariate analyses from MOZAIC data, *Atmos. Environ.*, *36*, 1123–1135.

Boucouvala, D., and R. Bornstein (2003), Analysis of transport patterns during and SCOS97-NARSTO episode, *Atmos. Environ.*, *37*, 73–94.

Byun, D. W., , and J. K. S. Ching (Eds.) (1999), Science algorithms of the EPA Models-3 Community Multiscale Air Quality (CMAQ) Modeling System, *EPA Rep. EPA-600/R-99/030*, Off. of Res. and Dev., U.S. Environ. Prot. Agency, Washington, D. C.

Coll, I., S. Pinceloup, P. E. Perros, G. Laverdet, and G. Le Bras (2005), 3D analysis of high ozone production rates observed during the ESCOMPTE campaign, *Atmos. Res.*, *74*, 477–505.

Cousin, F., P. Tulet, and R. Rosset (2005), Interaction between local and regional pollution during ESCOMPTE 2001: Impact on surface ozone concentrations (IOP2a and 2b), *Atmos. Res.*, *74*, 117–137.

Cros, B., et al. (2004), The ESCOMPTE program: An overview, *Atmos. Res.*, *69*, 241–279.

Dabdub, D., L. L. DeHaan, and J. H. Seinfeld (1999), Analysis of ozone in the San Joaquin Valley of California, *Atmos. Environ.*, *33*, 2501–2514.
Danielsen, E., and V. Mohnen (1977), Ozone transport, in situ measurements and meteorological analyses of tropopause foldings, *J. Geophys. Res.*, *82*, 5867–5877.
Draxler, R. R., and G. D. Hess (1998), An overview of the Hysplit_4 modelling system for trajectories, dispersion, and deposition, *Aust. Meteorol. Mag.*, *47*, 295–308.
Duclau, O., et al. (2002), 3D-air quality model evaluation using the Lidar technique, *Atmos. Environ.*, *36*, 5081–5095.
Dudhia, J. (1993), A nonhydrostatic version of the Penn State/NCAR mesoscale model: Validation tests and simulation of an Atlantic cyclone and cold front, *Mon. Weather Rev.*, *121*, 1493–1513.
Dueñas, C., M. C. Fernández, S. Cañete, J. Carretero, and E. Liger (2002), Assessment of ozone variations and meteorological effects in an urban area in the Mediterranean coast, *Sci. Total Environ.*, *299*, 97–113.
Dufour, A., M. Amodei, G. Ancellet, and V.-H. Peuch (2005), Observed and modelled chemical weather during ESCOMPTE, *Atmos. Res.*, *74*, 161–189.
Duncan, B. N., and I. Bey (2004), A modeling study of the export pathways of pollution from Europe: Seasonal and interannual variations (1987–1997), *J. Geophys. Res.*, *109*, D08301, doi:10.1029/2003JD004079.
Ellrod, G., and D. Knapp (1992), An objective clean-air turbulence forecasting technique: Verification and operational use, *Weather Forecast*, *7*, 150–165.
Fischer, H., et al. (2003), Deep convective injection of boundary layer air into the lowermost stratosphere at midlatitudes, *Atmos. Chem. Phys.*, *3*, 739–745.
Gangoiti, G., M. M. Millán, R. Salvador, and E. Mantilla (2001), Long-range transport and re-circulation of pollutants in the western Mediterranean during the project regional cycles of air pollution in the west-central Mediterranean area, *Atmos. Environ.*, *35*, 6267–6276.
Ganzeveld, L. N., J. Lelieveld, and G. J. Roelofs (1998), A dry deposition parameterization for sulfur oxides in a chemistry-general circulation model, *J. Geophys. Res.*, *103*, 5679–5694.
Gery, M. W., G. Z. Whitten, J. P. Killus, and M. C. Dodge (1989), A photochemical kinetics mechanism for urban and regional scale computer modelling, *J. Geophys. Res.*, *94*(D10), 12,925–12,956.
Hauf, T., P. Schulte, R. Alheit, and H. Schlager (1995), Rapid vertical transport by an isolated midlatitude thunderstorm, *J. Geophys. Res.*, *100*, 22,957–22,970.
Hauglustaine, D. A., and G. P. Brasseur (2001), Evolution of tropospheric ozone under anthropogenic activities and associated radiative forcing on climate, *J. Geophys. Res.*, *106*, 32,337–32,360.
Hoerling, M., T. Schaak, and A. Lenzen (1991), Global objective tropopause analysis, *Mon. Weather Rev.*, *119*, 1816–1839.
Huang, H.-C., and J. S. Chang (2001), On the performance of numerical solvers for a chemistry submodel in three-dimensional air quality models, *J. Geophys. Res.*, *106*, 20,175–20,188.
Jacobson, M. Z. (2002), *Atmospheric Pollution: History, Science and Regulation*, 412 pp., Cambridge Univ. Press, New York.
Jang, C. J., H. E. Jeffries, D. Byun, and J. E. Pleim (1995), Sensitivity of ozone to model grid resolution—II. Detailed process analysis for ozone chemistry, *Atmos. Environ.*, *29*(21), 3101–3114.
Jian, G., B. Lamb, and H. Westberg (2003), Using back trajectories and process analysis to investigate photochemical ozone production in the Puget Sound region, *Atmos. Environ.*, *37*, 1489–1502.
Jiménez, P., C. Pérez, A. Rodríguez, and J. M. Baldasano (2003a), Correlated levels of particulate matter and ozone in the western Mediterranean basin: Air quality and lidar measurements, paper presented at 22nd Annual Conference, Am. Assoc. for Aerosol Res., Anaheim, Calif.
Jiménez, P., D. Dabdub, and J. M. Baldasano (2003b), Comparison of photochemical mechanisms for air quality modelling, *Atmos. Environ.*, *37*, 4179–4194.
Jiménez, P., R. Parra, and J. M. Baldasano (2005a), Modeling the ozone weekend effect in very complex terrains: A case study in the northeastern Iberian Peninsula, *Atmos. Environ.*, *39*, 429–444.
Jiménez, P., O. Jorba, R. Parra, and J. M. Baldasano (2005b), Influence of high-model grid resolution on photochemical modeling in very complex terrains, *Int. J. Environ. Pollut.*, *24*(1–4), 180–200.
Jöckel, P., R. Sander, A. Kerkweg, H. Tost, and J. Lelieveld (2005), Technical Note: The Modular Earth Submodel System (MESSy)—A new approach towards Earth system modeling, *Atmos. Chem. Phys.*, *5*, 433–444.
Jorba, O., C. Pérez, F. Rocadenbosch, and J. M. Baldasano (2004), Cluster analysis of 4-day back trajectories arriving in the Barcelona area (Spain) from 1997 to 2002, *J. Appl. Meteorol.*, *43*(6), 887–901.
Kalthoff, N., C. Kottmeier, J. Thürauf, U. Corsmeier, F. Saïd, E. Frejafon, and P. E. Perros (2005), Mesoscale circulation systems and ozone concentrations during ESCOMPTE: A case study from IOP2b, *Atmos. Res.*, *74*, 355–380.
Kentarchos, A. S., and G. J. Roelofs (2003), A model study of stratospheric ozone in the troposphere and its contribution to tropospheric OH formation, *J. Geophys. Res.*, *108*(D12), 8517, doi:10.1029/2002JD002598.
Lasry, F., I. Coll, and E. Buisson (2005), An insight into the formation of severe ozone episodes: Modelling the 21/03/01 event in the ESCOMPTE region, *Atmos. Res.*, *74*, 191–215.
Lawrence, M. G., P. J. Crutzen, P. J. Rasch, B. E. Eaton, and N. M. Mahowald (1999), A model for studies of tropospheric photochemistry: Description, global distributions and evaluation, *J. Geophys. Res.*, *104*, 26,245–26,277.
Lelieveld, J., and F. J. Dentener (2000), What controls tropospheric ozone?, *J. Geophys. Res.*, *105*, 3531–3551.
Lelieveld, J., et al. (2002), Global air pollution crossroads over the Mediterranean, *Science*, *298*, 794–799.
Lin, S. J., and R. B. Rood (1996), Multidimensional flux form semi-Lagrangian transport, *Mon. Weather Rev.*, *124*, 2046–2068.
Liu, S. C., M. Trainer, F. C. Fehsenfeld, D. D. Parrish, E. J. Williams, D. W. Fahey, G. Hübler, and P. C. Murphy (1987), Ozone production in the rural troposphere and the implications for regional and global ozone distributions, *J. Geophys. Res.*, *92*, 4191–4207.
Lu, R., and R. P. Turco (1996), Ozone distributions over the Los Angeles basin: Three-dimensional simulations with the smog model, *Atmos. Environ.*, *30*, 4155–4176.
McElroy, J. L., and T. B. Smith (1993), Creation and fate of ozone layers aloft in Southern California, *Atmos. Environ.*, *27*, 1917–1929.
Millán, M. M., B. Artiñano, L. Alonso, M. Castro, R. Fernandez-Patier, and J. Goberna (1992), Mesometeorological cycles of air pollution in the Iberian Peninsula, *Air Pollut. Res. Rep. 44*, 219 pp., Comm. of the Eur. Commun., Brussels.
Millán, M. M., R. Salvador, E. Mantilla, and B. Artíñano (1996), Meteorology and photochemical air pollution in southern Europe: Experimental results from EC research projects, *Atmos. Environ.*, *30*, 1909–1924.
Millán, M. M., R. Salvador, and E. Mantilla (1997), Photooxidant dynamics in the Mediterranean basin in summer: Results from European research projects, *J. Geophys. Res.*, *102*(D7), 8811–8823.
Millán, M. M., E. Mantilla, R. Salvador, A. Carratala, M. J. Sanz, L. Alonso, G. Gangoiti, and M. Navazo (2000), Ozone cycles in the western Mediterranean basin: Interpretation of monitoring data in complex coastal terrain, *J. Appl. Meteorol.*, *4*, 487–507.
Ntziachristos, L., and Z. Samaras (2000), COPERTIII Computer programme to calculate emissions from road transport. Methodology and emission factors (version 2.1), *Tech. Rep. 49*, Eur. Environ. Agency, Copenhagen.
O'Connor, F. M., K. S. Law, J. A. Pyle, H. Barjat, N. Brough, K. Dewey, T. Green, J. Kent, and G. Phillips (2004), Tropospheric ozone budget: Regional and global calculations, *Atmos. Chem. Phys. Disc.*, *4*, 991–1036.
Parra, R., S. Gassó, and J. M. Baldasano (2004), Estimating the biogenic emissions of non-methane volatile organic compounds from the north-western Mediterranean vegetation of Catalonia, Spain, *Sci. Total Environ.*, *329*, 241–259.
Parra, R., P. Jiménez, and J. M. Baldasano (2006), Development of the high spatial resolution EMICAT2000 emission model for air pollutants from the north-eastern Iberian Peninsula (Catalonia, Spain), *Environ. Pollut.*, *140*, 200–219.
Pérez, C., M. Sicard, O. Jorba, A. Comerón, and J. M. Baldasano (2004), Summertime re-circulations of air pollutants over the north-eastern Iberian coast observed from systematic EARLINET lidar measurements in Barcelona, *Atmos. Environ.*, *38*, 3983–4000.
Reed, R. (1955), A study of a characteristic type of upper level frontogenesis, *J. Meteorol.*, *12*, 226–237.
Ribas, A., and J. Peñuelas (2004), Temporal patterns of surface ozone levels in different habitats of the northwestern Mediterranean basin, *Atmos. Environ.*, *38*, 985–992.
Roeckner, E., et al. (2003), The atmospheric general circulation model ECHAM5: Model description, *MPI Rep. 349*, 127 pp., Max-Planck-Inst. for Meteorol., Hamburg, Germany.
Roelofs, G. J., and J. Lelieveld (1995), Distribution and budget of O_3 in the troposphere calculated with a chemistry-general circulation model, *J. Geophys. Res.*, *100*, 20,983–20,998.
Roelofs, G. J., and J. Lelieveld (2000), Tropospheric ozone simulation with a global chemistry-climate model: Influence of higher hydrocarbon chemistry, *J. Geophys. Res.*, *105*, 22,697–22,712.
Roelofs, G. J., H. A. Scheeren, J. Heland, H. Ziereis, and J. Lelieveld (2003), A model study of ozone in the eastern Mediterranean free troposphere during MINOS (August 2001), *Atmos. Chem. Phys.*, *3*, 1199–1210.
Russell, A., and R. Dennis (2000), NARSTO critical review of photochemical models and modeling, *Atmos. Environ.*, *34*, 2283–2324.
Sander, R., and P. J. Crutzen (1996), Model study indicating halogen activation and ozone destruction in polluted air masses transported to the sea, *J. Geophys. Res.*, *101*, 9121–9138.

Sander, R., A. Kerkweg, P. Jöckel, and J. Lelieveld (2005), Technical Note: The new comprehensive atmospheric chemistry module MECCA, *Atmos. Chem. Phys.*, *5*, 445–450.

Sicard, M., C. Pérez, F. Rocadenbosch, J. M. Baldasano, and D. García-Vizcaino (2006), Mixed-layer depth determination in the Barcelona coastal area from regular lidar measurements: Methods, results and limitations, *Boundary Layer Meteorol.*, *119*(1), 135–157.

Soriano, C., J. M. Baldasano, W. T. Buttler, and K. Moore (2001), Circulatory patterns of air pollutants within the Barcelona air basin in a summertime situation: Lidar and numerical approaches, *Boundary Layer Meteorol.*, *98*(1), 33–55.

Steil, B., M. Dameris, C. Brühl, P. J. Crutzen, V. Grewe, M. Ponater, and R. Sausen (1998), Development of a chemistry module for GMCs: First results of a multiannual integration, *Ann. Geophys.*, *16*, 205–228.

Stohl, A., and T. Trickl (1999), A textbook example of long-range transport: Simultaneous observation of ozone maxima of stratospheric and North American origin in the free troposphere over Europe, *J. Geophys. Res.*, *104*(D32), 30,445–30,462.

Ström, J., H. Fischer, J. Lelieveld, and F. Schröder (1999), In situ measurements of aerosol microphysical properties and trace gases in two cumulonimbus anvils over western Europe, *J. Geophys. Res.*, *104*, 12,221–12,226.

Toll, I., and J. M. Baldasano (2000), Modeling of photochemical air pollution in the Barcelona area with highly disaggregated anthropogenic and biogenic emissions, *Atmos. Environ.*, *34*(19), 3060–3084.

Traub, M., and J. Lelieveld (2003), Cross-tropopause transport over the eastern Mediterranean, *J. Geophys. Res.*, *108*(D23), 4712, doi:10.1029/2003JD003754.

Traub, M., et al. (2003), Chemical characteristics assigned to trajectory clusters during the MINOS campaign, *Atmos. Chem. Phys.*, *3*, 459–468.

Tulet, P., K. Suhre, C. Mari, F. Solmon, and R. Rosset (2002), Mixing of boundary layer and upper tropospheric ozone during a deep convective event over Western Europe, *Atmos. Environ.*, *36*, 4491–4501.

U.S. Environmental Protection Agency (1991), Guideline for regulatory application of the Urban airshed model, *U.S. EPA Rep. EPA-450/4-91-013*, Off. of Air and Radiat., Off. of Air Qual. Plann. and Stand., Tech. Support Div., Research Triangle Park, N. C.

U.S. Environmental Protection Agency (2005), Guidance on the use of models and other analyses in attainment demonstrations for the 8-hour ozone NAAQS, *U.S. EPA Rep. EPA-454/R-05-002*, 128 pp., Off. of Air Qual. Plann. and Stand., Research Triangle Park, N. C.

van Aardenne, J. A., F. J. Dentener, J. G. J. Olivier, C. M. G. Klein-Goldewijk, and J. Lelieveld (2001), A $1^\circ \times 1^\circ$ resolution data set of historical anthropogenic trace gas emissions for the period 1890–1990, *Global Biogeochem. Cycles*, *15*(4), 909–928.

von Glasow, R., R. Sander, A. Bott, and P. J. Crutzen (2002), Modeling halogen chemistry in the marine boundary layer 1. Cloud-free MBL, *J. Geophys. Res.*, *107*(D17), 4341, doi:10.1029/2001JD000942.

von Kuhlmann, R., M. G. Lawrence, P. J. Crutzen, and P. J. Rasch (2003), A model for studies of tropospheric ozone and nonmethane hydrocarbons: Model description and ozone results, *J. Geophys. Res.*, *108*(D9), 4294, doi:10.1029/2002JD002893.

Wakimoto, R. M., and J. L. McElroy (1986), Lidar observation of elevated pollution layers over Los Angeles, *J. Clim. Appl. Meteorol.*, *25*, 1583–1599.

Wang, Y., D. J. Jacob, and J. A. Logan (1998), Global simulation of tropospheric O_3-NO_x-hydrocarbon chemistry: 2. Model evaluation and global ozone budget, *J. Geophys. Res.*, *103*, 10,727–10,755.

Wild, O., and H. Akimoto (2001), Intercontinental transport of ozone and its precursors in a three-dimensional global CTM, *J. Geophys. Res.*, *106*, 27,729–27,744.

Wirth, V. (1995a), Comments on "A new formulation of the exchange of mass and trace constituents between the stratosphere and troposphere", *J. Atmos. Sci.*, *53*, 2491–2493.

Wirth, V. (1995b), Diabatic heating in an axisymmetric cut-off cyclone and related stratosphere-troposphere exchange, *Q. J. R. Meteorol. Soc.*, *121*, 127–147.

Ziomas, I. C., S. E. Gryning, and R. D. Borsteing (1998), The Mediterranean campaign of photochemical tracers-transport and chemical evolution (MEDCAPHOT-TRACE), *Atmos. Environ.*, *32*, 2043–2326.

J. M. Baldasano and P. Jiménez, Barcelona Supercomputing Center–Centro Nacional de Supercomputación, Jordi Girona 29, Edificio Nexus II, E-08034 Barcelona, Spain. (pedro.jimenez@bsc.es)

J. Lelieveld, Department of Atmospheric Chemistry, Max Planck Institute for Chemistry, Joh.-J.-Becher-Weg 27, D-55128 Mainz, Germany.